Am J Cancer Res 2023;13(3):778-801
www.ajcr.us /ISSN:2156-6976/ajcr0148145

*Original Article*

# Characterization of cuproptosis-related lncRNA landscape for predicting the prognosis and aiding immunotherapy in lung adenocarcinoma patients

Xinti Sun[1,2*], Jiaming Song[3*], Chenglu Lu[4*], Xiaojun Sun[5], Haoran Yue[2], Hongxin Bao[6], Siben Wang[7], Xugang Zhong[1,8]

*[1]Department of Orthopedics, Zhejiang Provincial People's Hospital, Hangzhou, Zhejiang, China; [2]Tianjin Medical University, Tianjin, China; [3]Tianjin Key Laboratory of Lung Cancer Metastasis and Tumor Microenvironment, Lung Cancer Institute, Tianjin, China; [4]Department of Pathology, Tianjin Medical University Cancer Institute and Hospital, Tianjin, China; [5]Department of Oncology, Qingdao University Affiliated Hospital, Qingdao, Shandong, China; [6]Inner Mongolia Agricultural University, Hohhot, Inner Mongolia, China; [7]The First Hospital of Anhui University of Science & Technology, Huainan, Anhui, China; [8]Qingdao University, Qingdao, Shandong, China. [*]Equal contributors and co-first authors.*

Received November 30, 2022; Accepted February 5, 2023; Epub March 15, 2023; Published March 30, 2023

**Abstract:** Cuproptosis is a newly discovered mechanism of regulated cell death, which serves as a novel target for cancer therapy. Long non-coding RNAs (lncRNAs) play an important role in the initiation and progression of cancer cells; however, the relationship between cuproptosis and lncRNAs in tumorigenesis and cancer treatment has not been well established in lung adenocarcinoma (LUAD). Thus, it is important to clarify and characterize the cuproptosis-related lncRNA landscape in LUAD. In this study, cuproptosis-related lncRNAs was screened by Pearson correlation analysis. Then, univariate, Least Absolute Shrinkage and Selection Operator (LASSO), and multivariate Cox regression were conducted to identify 6 cuproptosis-related lncRNAs (AC090541.1, AC009226.1, NIFK-AS1, AC027097.2, AC026355.2, and AC106028.2) which were used to construct a cuproptosis-related lncRNA signature (CRLS). Multi-dimensional assessments including Kaplan-Meier analysis, receiver operating characteristics (ROC) curves, and principal component analysis (PCA) verified that the CRLS could reliably predict the prognosis and survival of LUAD patients. We further compared the immune cell infiltration, somatic mutation landscape, and functional enrichment pathways between the high and low CRLS groups. Patients with low CRLS scores had prolonged survival and were sensitive to immunotherapy, whereas patients with high CRLS scores might benefit better from chemotherapy. We further analyzed the individualized immunotherapeutic strategies and the candidate compounds for the potential clinical treatment. Moreover, the expression level of these 6 lncRNAs was examined experimentally in vitro by using quantitative real-time polymerase chain reaction (RT-qPCR). Additionally, one of the significantly differentially expressed lncRNAs, NIFK-AS1, was confirmed to suppress the proliferation and migration of LUAD by Cell Counting Kit-8 Assays (CCK-8), wound healing assay, and colony formation assays. Taken together, we established a CRLS that might be a promising tool for predicting the prognosis, guiding individualized treatment, and serving as a promising therapeutic target for patients with LUAD.

**Keywords:** Lung adenocarcinoma, lncRNA, cuproptosis, immune therapy, bioinformatics

## Introduction

Lung cancer is one of the most malignant tumors worldwide, while lung adenocarcinoma (LUAD) is the most prevalent non-small cell lung cancer [1-5]. Despite the improvements in surgery, immunotherapy, and radiotherapy for the treatment of LUAD, the overall survival (OS) of LUAD patients remains low, with 5-year survival rates varying from 4 to 17% [6], mainly due to the lack of effective early detection of LUAD. Hence, it is urgent to identify biomarkers of LUAD to facility the diagnosis and hence improve the prognosis of LUAD [7].

Cuproptosis is a newly identified cooper-dependent form of regulated cell death (RCD) that is triggered by mitochondrial stress, particularly

by the polymerization of lipoylated mitochondrial enzymes, which is different from other forms of RCD such as apoptosis, ferroptosis, and autophagy [8, 9]. It has been reported that the copper-induced cell death is dependent on mitochondrial respiration, whereas ATP produced by glycolysis has less impact on it. The copper atom is not directly involved in the electron transport chain (ETC) but plays a role in the tricarboxylic acid cycle (TCA). It appears that copper-induced cell death and mitochondrial metabolism are closely related, and there is a strong link between copper and the TCA cycle [9]. Although the detailed mechanism underlying the role of cuproptosis in tumors is still unclear, the copper ionophore Elesclomol has already been used to treat cancer patients where tumor growth depends on mitochondria for energy [9].

Long non-coding RNAs (lncRNAs) are transcripts of more than 200 nucleotides that do not encode proteins [10]. Accumulating evidence has shown that lncRNAs contribute significantly to tumorigenesis by regulating cell death. For example, Yan et al. showed that specific lncRNAs could influence the ferroptosis process of cancers [11]. Similarly, Wang et al. found that lncRNA LIN0033 inhibited ferroptosis in LUAD [12], and lncRNA FAM207BP was reported to promote the tumorigenesis and metastasis of LUAD [13]. In addition, P53RRA induces tumor suppression via nuclear sequestration of p53 to promote ferroptosis and apoptosis in cancer cells [14]. However, the lncRNA regulation of cuproptosis in LUAD is unknown.

Herein, we comprehensively investigated the clinical value of cuproptosis and lncRNA expression profiles in LUAD, and a signature based on cuproptosis-related lncRNA named CRLS was established from the combination of univariate, LASSO, and multivariate Cox regression analyses. Furthermore, we developed and evaluated a nomogram to predict the prognosis of patients with LUAD. Moreover, we carried out comprehensive analyses including functional enrichment, immune cell infiltration, immunotherapy, drug sensitivity, and somatic mutation on patients with different CRLS scores to reveal the potential mechanism and guide clinical treatment. Importantly, we experimentally validated that the 6 lncRNAs that were used to generate the CRLS were differentially expressed between LUAD cell lines (A549, NCI-H1975) and normal cell line (BEAS2B) by using RT-qPCR. Finally, in vitro experiments demonstrated that the overexpression of NIFK-AS1, one of the 6 lncRNAs in CRLS, suppressed the proliferation and migration of LUAD cells. Taken together, our findings may help predict the prognosis, provide guidance in treatment decision-making, and shed light on the possible mechanism of cuproptosis-related lncRNAs in LUAD.

## Methods

### *Data acquisition*

RNA sequencing data, somatic mutations, and the corresponding clinical information of LUAD samples were obtained from TCGA database (http://portal.gdc.cancer.gov/). The UCSC's Xena program (http://xena.ucsc.edu/) was used to obtain the copy number variation (CNV) data. To ensure the authenticity of the analysis results, we excluded the samples without survival information or with survival time of less than 30 days. At the end, 490 patients were included in this study and were randomly divided into training (n = 246) and testing (n = 244) sets using the R package "*caret*". The Chi-square tests were performed to compare the clinical characteristics between the training and testing sets.

### *Identification of cuproptosis-related lncRNAs*

We selected 10 cuproptosis-related genes (CRGs) through literature review [9] (Table S1). To identify cuproptosis-related lncRNAs, 14056 lncRNAs were extracted according to the annotation file of lncRNA obtained from the GENCODE database (https://www.gencodegenes.org/human/) using the "*Perl*" language, and 852 cuproptosis-related lncRNAs were identified through Pearson's correlation analysis (|Pearson R| > 0.4, $P < 0.001$).

### *Construction of the CRLS*

The training set was employed to construct the CRLS, while the testing and the entire sets were applied to validate the predictive ability of the established CRLS. Univariate Cox regression ($P < 0.05$), LASSO regression (employing the penalty parameter determined through 10-fold cross-validation) [15], and multivariate Cox regression [16] analyses were applied to ana-

lyze the prognostic lncRNAs using the "*glmnet*" package, Furthermore, the CRLS score of each LUAD patient was calculated using the formula:

CRLS score = ∑*Coef* lncRNAs × *Exp* lncRNAs

(Coef and Exp represent the coefficient and the expression level of CRL, respectively).

We then used the optimal cut-off value to divide the patients into high and low CRLS groups as determined by the "*survminer*" package.

*Assessment of the CRLS and construction of a nomogram*

Kaplan-Meier (K-M) analysis was conducted to assess the performance of the CRLS using the R package "*survival*". In addition, the Receiver operating characteristics (ROC) curve was drawn to demonstrate the predictive power of the CRLS using the package "*timeROC*". Principal component analysis (PCA) [17] was further conducted to lessen the dimensions and visualize the distinction between the two groups. Independent prognostic factor analysis using univariate Cox and multivariate Cox regression was conducted in R with package "*survival*". A nomogram was created to better predict survival by using "*RMS*" packages in R. The concordance index (C-index) and calibration plot were carried out to test the accuracy of our nomogram.

*Analysis of immune cell infiltration and molecular variation*

CIBERSORT, TIMER, xCELL, quanTIseq, MCP-counter, EPIC, CIBESORT-ABS, [18] and ssGSEA [19] algorithms were applied to estimate the infiltration level of immune cell populations. The ESTIMATE algorithm was applied to investigate the relationship among immune, stromal, estimate scores, and the CRLS. We analyzed tumor mutation burden (TMB) using the package "*maftools*" and divided all LUAD patients into high and low TMB groups according to the median TMB score. Furthermore, we calculated the correlation between the CRLS and TMB by Spearman correlation analysis.

*Drug sensitivity and immunotherapeutic response prediction*

To explore the potential clinical application of the CRLS, we calculated the half-maximal inhibitory concentration (IC50) values of common anti-tumor drugs by using the R package "*pRRophetic*" based on the Genomics of Drug Sensitivity in Cancer (GDSC) database (https://www.cancerrxgene.org/). The prediction process was estimated via ridge regression and the prediction accuracy was evaluated with 10-fold cross-validation. The "*ImmuneSubtypeClassifier*" package was used to calculate the immune subtypes for each sample. The TIMER 2.0 web site (http://timer.cistrome.org/) was used to analyze the immune cell infiltration of samples from the TCGA database [20]. The immunophenotypic scores (IPS) of LUAD was obtained from The Cancer Imaging Archive (TCIA) database (https://tcia.at/home), and the differences in all kinds of IPS between the two groups were calculated using the Wilcoxon rank sum test. To investigate the potential application of the CRLS in immunotherapy prediction, we also compared the expression profiles of checkpoint members between two groups.

*Functional enrichment analysis*

The differentially expressed genes (DEGs) between low and high CRLS groups were identified by using the package "*limma*" following the criteria |Log2FC| > 2.0, *P*-value < 0.05. GO, KEGG, and DO enrichment analyses were performed using the package "clusterProfiler". GSEA analysis was conducted to screen functional pathways, and "c2.cp.kegg *v7.4.symbols.gmt*" was used as the reference file. FDR < 0.05 was considered statistically significant. Sankey diagram was used to visualize the correlation among CRGs, cuproptosis-related lncRNAs, and risk factors (protective/risk) using the R package "*ggalluvial*".

*Cell culture*

Human LUAD cell lines A549 and NCI-H1975 as well as normal lung epithelial cell line BEAS-2B were purchased from the America Type Culture Collection (Manassas, VA, USA) and were culture in RPMI-1640 medium supplemented with 10% fetal bovine serum in 5% $CO_2$ at 37°C.

*Total RNA extraction and real-time quantitative PCR*

To assess the expression levels of 6 lncRNAs, total RNA was isolated from cells using Trizol reagent (Invitrogen, Carlsbad, CA, USA). The PrimeScriptTM RT Reagent Kit (Takara, Dalian,

Liaoning, China) was used to reverse transcribe total RNA according to the manufacturer's instructions. The cDNA was subjected to RT-qPCR using the ABI 7900HT platform (Applied Biosystems, USA). The relative expressions of the 6 lncRNAs were normalized to GAPDH. The primer sequences are shown in Table S7.

*Transfection*

NIFK-AS1 overexpression plasmids (pcDNA-3.1(+) ZB02427, Hind III/Xho I, 5'-GGGCGTCCG GTGTGTATA-3') were kindly provided by Sangon Biotech and transfected into cell lines using Lipofectamine 6000. The efficacy of NIFK-AS1 overexpression was assessed using RT-qPCR. Briefly, 100 pmol NIFK-AS1-expressing plasmid was mixed with 5 μl Lipofectamine 6000 for 5 minutes, and then the mixture was added to overnight-cultured A549 cells. At 24 h after transfection, the cells were replaced with regular medium, and the cells were collected at 48 h after transfection. Total RNA was extracted and subjected to RT-qPCR to examine the mRNA level of NIFK-AS1 as described above. RT-qPCR was conducted with the following oligonucleotide primers: NIFK-AS1: (forward 5'-CCATGTTTCCCAGCCTTGTC-3', reverse 5'-TGCATCTCAACACATCAAATTACC-3'); and GAPDH: (forward 5'-GGTGGTCTCCTCTCTCAACA-3', reverse 5'-GTTGCTGTAGCCAAATTCGTTGT-3'). The following RT-qPCR condition was used: 95°C for 10 minutes, 40 cycles of amplification (15 seconds at 95°C, 40 seconds at 60°C, 1 minute at 72°C), and extension (72°C for 2 minutes). All samples were examined in triplicates.

*Cell counting kit-8 assays*

CCK-8 assay (Dojindo, CK04) was used to examine the effect of NIFK-ASI overexpression on the proliferation of A549 cells. Briefly, cells were seeded in 96-well plates at the density of 6×10*3 cells per well. At 0, 24, 48, 72, and 96 h after culture, the CCK-8 cell proliferation reagent (20 μl) was added to each well, and the cells were cultured for another 2 h. A Microplate Spectrophotometer (BioTek, VT, USA) was used to measure the absorbance of the culture medium with cells at 450 nm.

*Wound healing assay*

Cells (7×10*5/well) were seeded in a 6-well plate and cultured for 24 h. A 20 μl pipette tip was then used for wound scratching. After rinsing with PBS twice, RPMI-1640 medium with 4% FBS was added to the cells. The images of the wound area were photographed at time 0 and 36 h after scratching. The width of the wound area was then measured and quantitated with Photoshop.

*Colony formation assays*

Transfected A549 cells were seeded in 6-well plates (5*10^3 or 5*10^2/well) and cultured continuously for 12 days. Then, the cells were fixed with 4% paraformaldehyde solution and then stained with 0.1% crystal violet (Beyotime Biotechnology) to detect the colony formation.

*Statistical analysis*

All statistical analyses were conducted in the *R*, *Perl*, and *GraphPad Prism 8* platforms. Student's t-test and Wilcoxon rank sum test were applied to determine the difference between two groups. The relationship between two variables was analyzed by Pearson's correlation and Spearman's correlation methods. To determine the differences between K-M curves, the log-rank test was performed. If no special instructions were given for the above methods of analysis, $P < 0.05$ was considered statistically significant.

## Results

*The landscape of CRGs and cuproptosis-related LncRNAs in LUAD*

The flowchart this study is displayed in **Figure 1**. First, we compared the expression levels of the 10 CRGs we selected between 59 normal and 535 LUAD tumor samples (**Figure 2A**). The results showed that, except for gene GLS, the other 9 CRGs were significantly differentially expressed between tumor and normal tissues. Heatmap also indicated the differential expression of them between normal and LUAD samples (**Figure 2B**). Furthermore, we explored the incidence of CNV mutations and found that these 10 CRGs harbored substantial CNV mutations. CDKN2A have decreased extensive CNVs, while MTF1, GLS, DLD, and LIPT1 presented an overall enhancement in the CNV (**Figure 2C**). **Figure 2D** depicts the locations of CNV alterations on chromosomes of 10 CRGs. Moreover, a PPI network using string websites

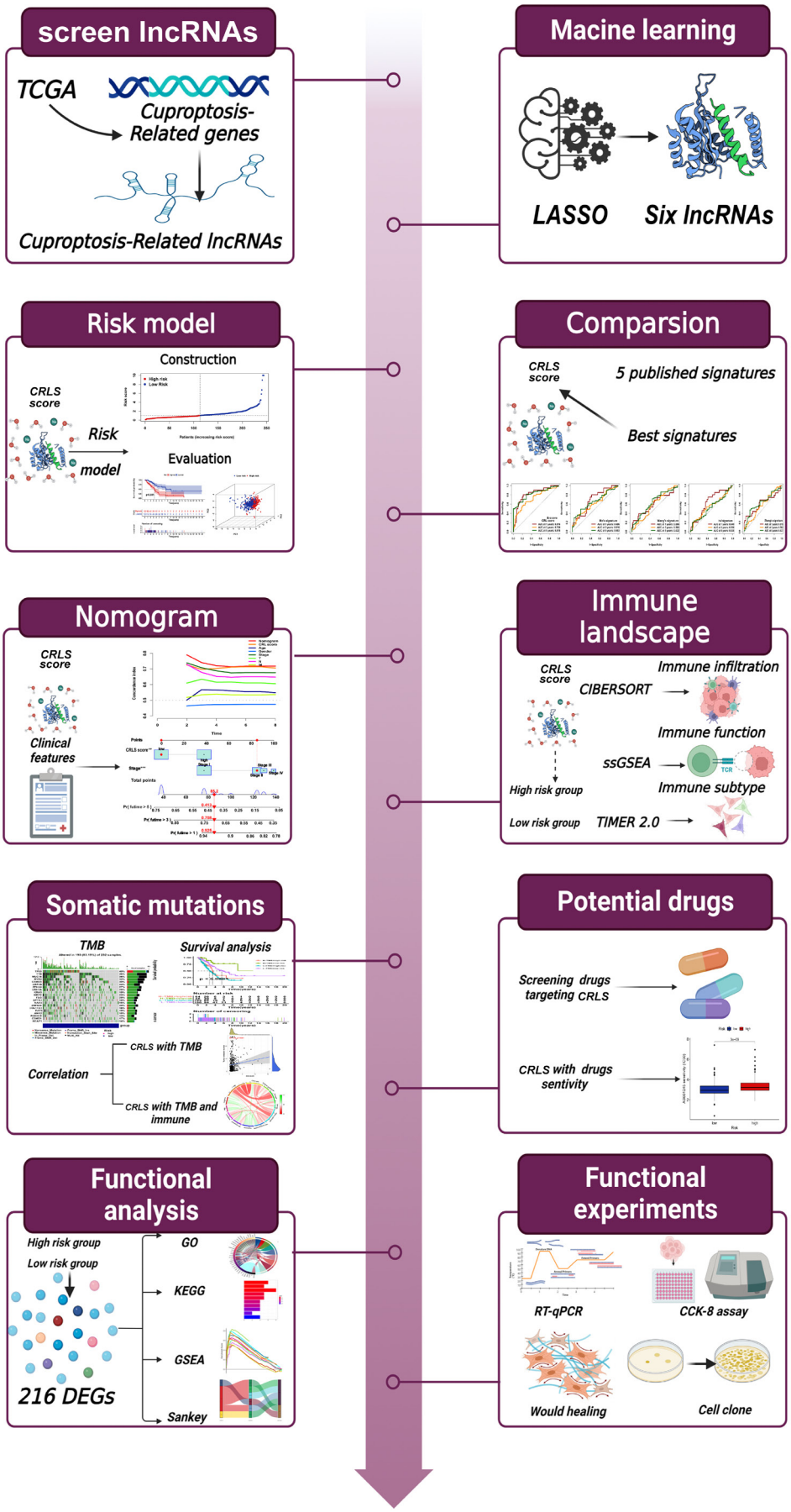
screen lncRNAs
TCGA
Cuproptosis-Related genes
Cuproptosis-Related lncRNAs
Macine learning
LASSO
Six lncRNAs
Risk model
Construction
CRLS score
Risk model
Evaluation
Comparsion
CRLS score
5 published signatures
Best signatures
Nomogram
CRLS score
Clinical features
Immune landscape
CRLS score
CIBERSORT
Immune infiltration
Immune function
ssGSEA
Immune subtype
High risk group
Low risk group
TIMER 2.0
Somatic mutations
TMB
Survival analysis
Correlation
CRLS with TMB
CRLS with TMB and immune
Potential drugs
Screening drugs targeting CRLS
CRLS with drugs sentivity
Functional analysis
High risk group
Low risk group
216 DEGs
GO
KEGG
GSEA
Sankey
Functional experiments
RT-qPCR
CCK-8 assay
Would healing
Cell clone

**Figure 1.** The workflow of this study. Datasets were obtained from public database, and Pearson correlation analysis was conducted to identify cuproptosis-related lncRNAs. Using multiple algorithms, the CRLS was constructed and proven to be a prognostic predictor of LUAD patients. A nomogram with high predictive accuracy combining the CRLS and the stage was then created. Then we conducted comprehensive analyses including tumor microenvironment, tumor mutation burden, potential drug screening, immune checkpoints, etc. Finally, in vitro experiments such as RT-qPCR, CCK8, wound healing assay, colony formation assays, etc. fully verified the function of hub lncRNA NIFK-AS1.

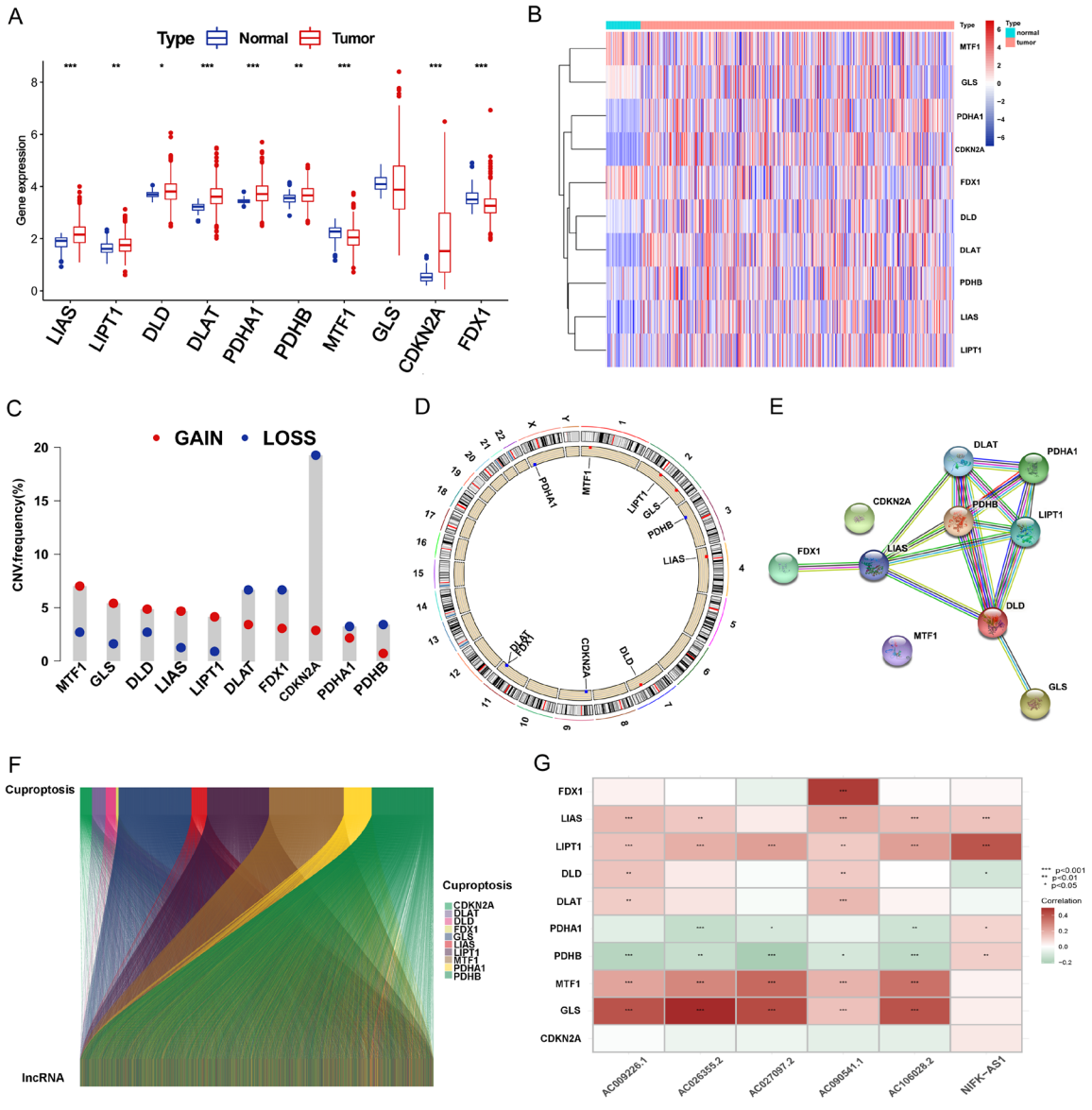


**Figure 2.** Genetic and expression variation of the CRGs in LUAD. A. Comparative analysis of normal and LUAD samples based on 10 CRGs. B. Expression distributions of CRGs between LUAD and normal tissues. C. The CNV frequency of 10 CRGs. D. Circus plots of 23 chromosome distributions of CRGs. E. The PPI network was acquired from the STRING database among the CRGs. F. Co-expression network in Sankey diagram for CRGs and corresponding lncRNAs. G. The heatmap of the correlation between 10 CAGs and 6 hub lncRNAs.

indicated that the 10 CRGs interacted closely with each other and that PDHB may be the hub gene (**Figure 2E**). Lastly, we performed Pearson correlation analysis with the criteria (|Pearson R| > 0.4 and $P < 0.001$) and identified 852 cuproptosis-related lncRNAs (Table S2). The CRGs-lncRNAs co-expression network was shown in the Sankey diagram (**Figure 2F**), and

the correlation between the CRGs and the hub cuproptosis-related lncRNAs was shown in the heatmap (**Figure 2G**).

*Construction of the CRLS*

In total, 490 patients with LUAD were included in the subsequent study, of which 246 patients were assigned to the training set, while 244 patients were in the testing set. The training test ws used to identify prognosis-associated lncRNAs and to further construct the CRLS which was validated in the testing set. We found that clinical characteristics such as age, stage, gender, and TNM are not statistically different between the two groups (Table S3, $P > 0.05$). A total of 11 cuproptosis-related lncRNAs were found highly related to prognosis by univariate Cox regression analysis (**Figure 3A**). In the LASSO regression analysis, the optimal lambda was identified when the partial likelihood deviance reached the minimum value, and 9 cuproptosis-related lncRNAs were significantly correlated with the prognosis of LUAD patients (**Figure 3B**, **3C**). Finally, 6 cuproptosis-related lncRNAs were selected by multivariate Cox regression analysis (**Figure 3D**, Table S4), and the CRLS score for each patient was subsequently calculated by the formula: *CRLS score* = 0.4878188777979 × expr AC090541.1 + -0.802318637135871 × expr AC027097.2 + 1.62072125434914 × expr AC009226.1 + -0.365560906490348 × expr AC026355.2 + 0.546026685241896 × expr NIFK-AS1 + -0.875355073859202 × expr AC106028.2.

Based on the optimal cut-off value determined by the "*survminer*" package, all patients were divided into high and low CRLS groups. We investigated the distribution of CRLS score in survival time and survival status between the high and low CRLS groups (**Figure 3E**, **3F**). Furthermore, we compared the expression of these six lncRNAs between the two groups (**Figure 3G**). Compared to patients with high CRLS scores, patients with low CRLS scores had significantly higher expression levels of CRLs including AC027097.2, AC026355.2, NIFK-AS1, and AC106028.2, which was consistent with their respective negative coefficients, indicating that they were protective factors. Additionally, we conducted the K-M analysis to determine whether the OS was significantly different between the high and low CRLS groups and found that LUAD patients in the low CRLS group had a better OS than patients in the high CRLS group (**Figure 3H**, $P < 0.001$). Consistently, PCA based on the CRLS showed a clear separation between two these CRLS groups (**Figure 3I**). Importantly, CRLS exhibited superior performance in the training set with time-dependent AUCs of 0.816, 0.720, and 0.818 at 1-, 3-, and 5-years, respectively (**Figure 3J**).

*Stable performance of CRLS*

We further verified the reliability and the predictive power of the established CRLS in the testing set. Using the same formula, the CRLS score for LUAD patients in the testing set was calculated. **Figure 4A-C** presented the CRLS score distributions, survival status, and the expressions of the 6 lncRNAs in the testing set. K-M analysis also showed that the LUAD patients with low CRLS scores had a better OS than the patients with high CRLS scores (**Figure 4D**, $P = 0.004$). PCA also revealed significant discrimination between the two groups (**Figure 4E**). The AUCs of 1-, 3-, and 5-year OS were 0.721, 0.65, and 0.60, respectively (**Figure 4F**). Furthermore, we used the entire set including 490 patients to confirm the predictive power of the established CRLS. Consistently, the entire set also manifested similar results as the aforementioned findings (**Figure 4G-L**). Importantly, we compared the CRLS with other published cuproptosis-related signatures in LUAD to assess the robustness of our signature. To exclude the impact of heterogeneity, only signatures developed based on TCGA database were retrieved; hence, 4 cuproptosis-related signatures including mRNA and lncRNA were included in the subsequent comparison (Table S5). We performed K-M analysis for each signature and found that all signatures including the CRLS were able to distinguish high risk and low risk LUAD patients in the entire set (**Figure 5A-E**, $P < 0.05$), and in the training set (Figure S1A-E). Additionally, we conducted the ROC curve analysis to evaluate the performance of these signatures and determined that our signature performed better than others, with time-dependent AUCs of 0.712, 0.664, and 0.690 at 1-, 3-, and 5-years, respectively, in the entire set (**Figure 5F-J**) and 0.816, 0.720, and 0.818, respectively, in the training set (Figure S1F-J).

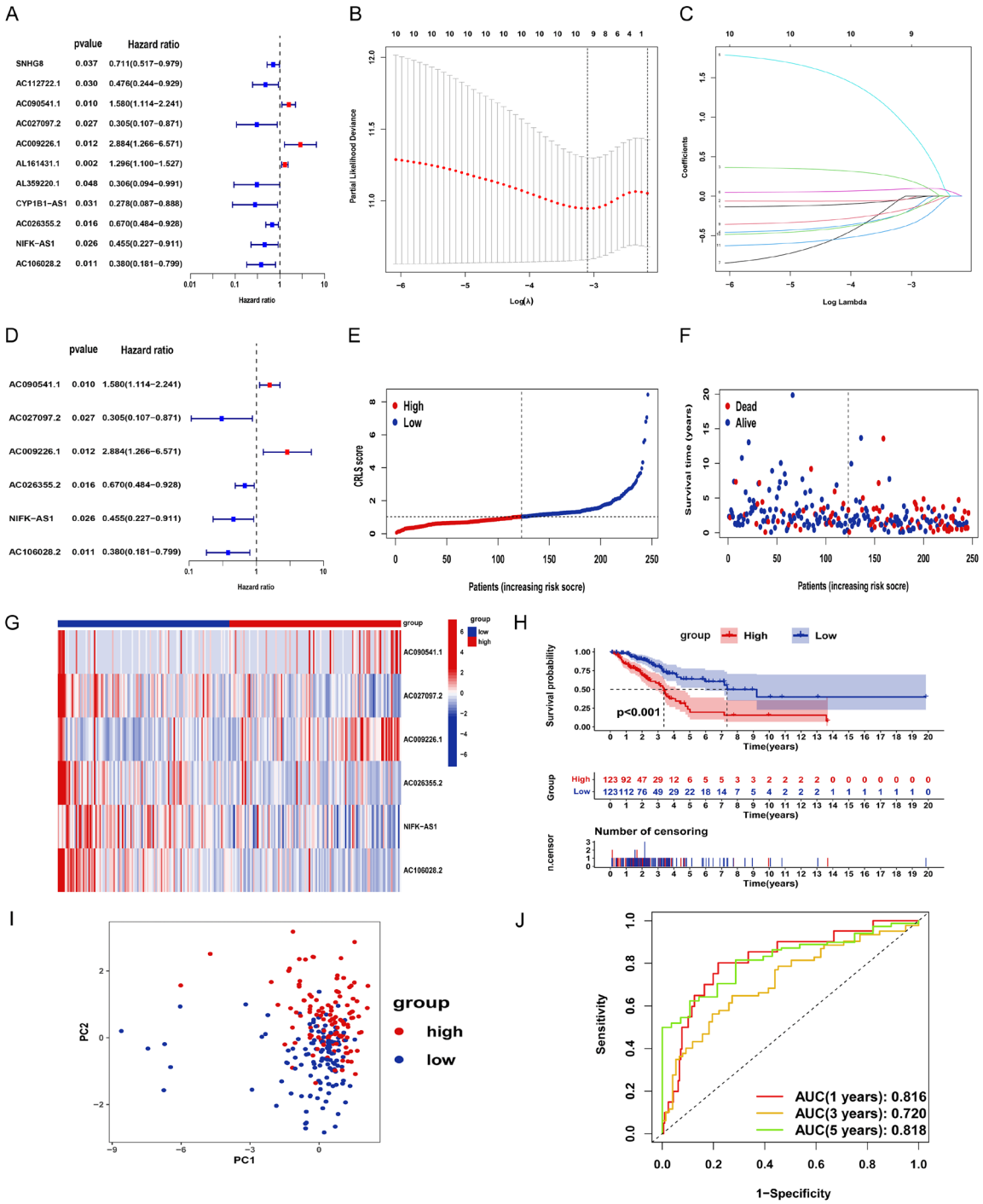


**Figure 3.** Construction and validation of the CRLS in the training set. (A) Univariate Cox regression analysis based on cuproptosis-related lncRNAs with survival status. (B, C) Ten-fold cross-validation by the LASSO Cox regression for the prognostic value of the cuproptosis-related lncRNAs. (D) Multivariate Cox regression analysis showed 6 cuproptosis-related lncRNAs. (E-J) Distribution of CRLS score (E), different patterns of survival status and survival time (F), clustering analysis heatmap of 6 lncRNAs (G), K-M survival curves (H), PCA (I), and ROC curve (J) for predicting 1-, 3-, and 5-years OS based on the training set.

Moreover, we applied PCA analysis to further verify the difference between the two groups according to the entire gene expression profiles of 10 CRGs, 852 cuproptosis-related lncRNAs,

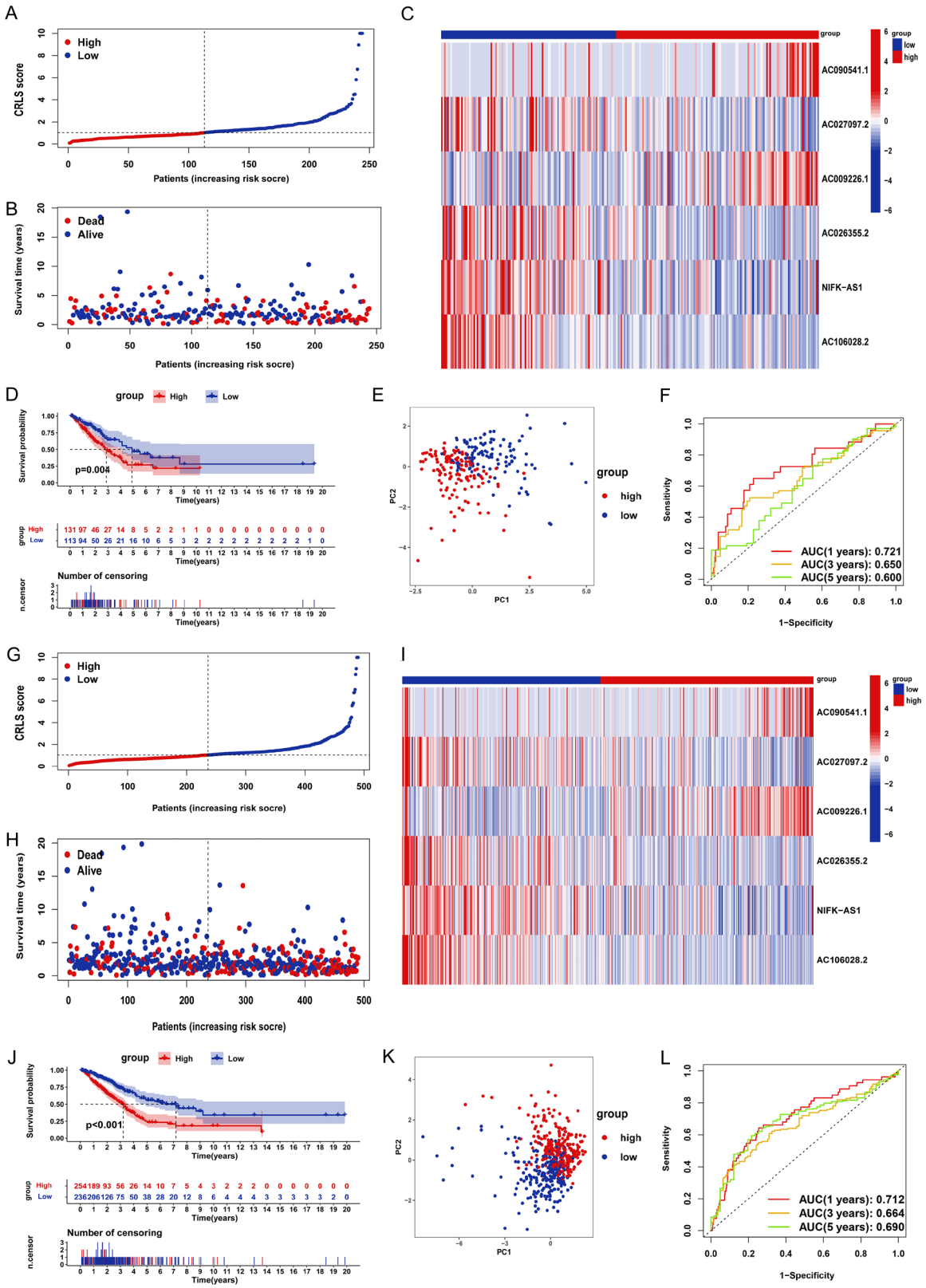


**Figure 4.** Prognostic value of the CRLS in the testing and entire sets. (A-F) Distribution of CRLS scores (A), survival time, and survival status patterns (B), the expression levels of six lncRNAs (C), K-M survival curve of OS (D), PCA (E), and ROC curve (F) based on the testing set. (G-L) Distribution of CRLS scores (G), survival time, and survival status patterns (H), the expression levels of six lncRNAs (I), K-M survival curve of OS (J), PCA (K), and ROC curve (L) based on the entire set.

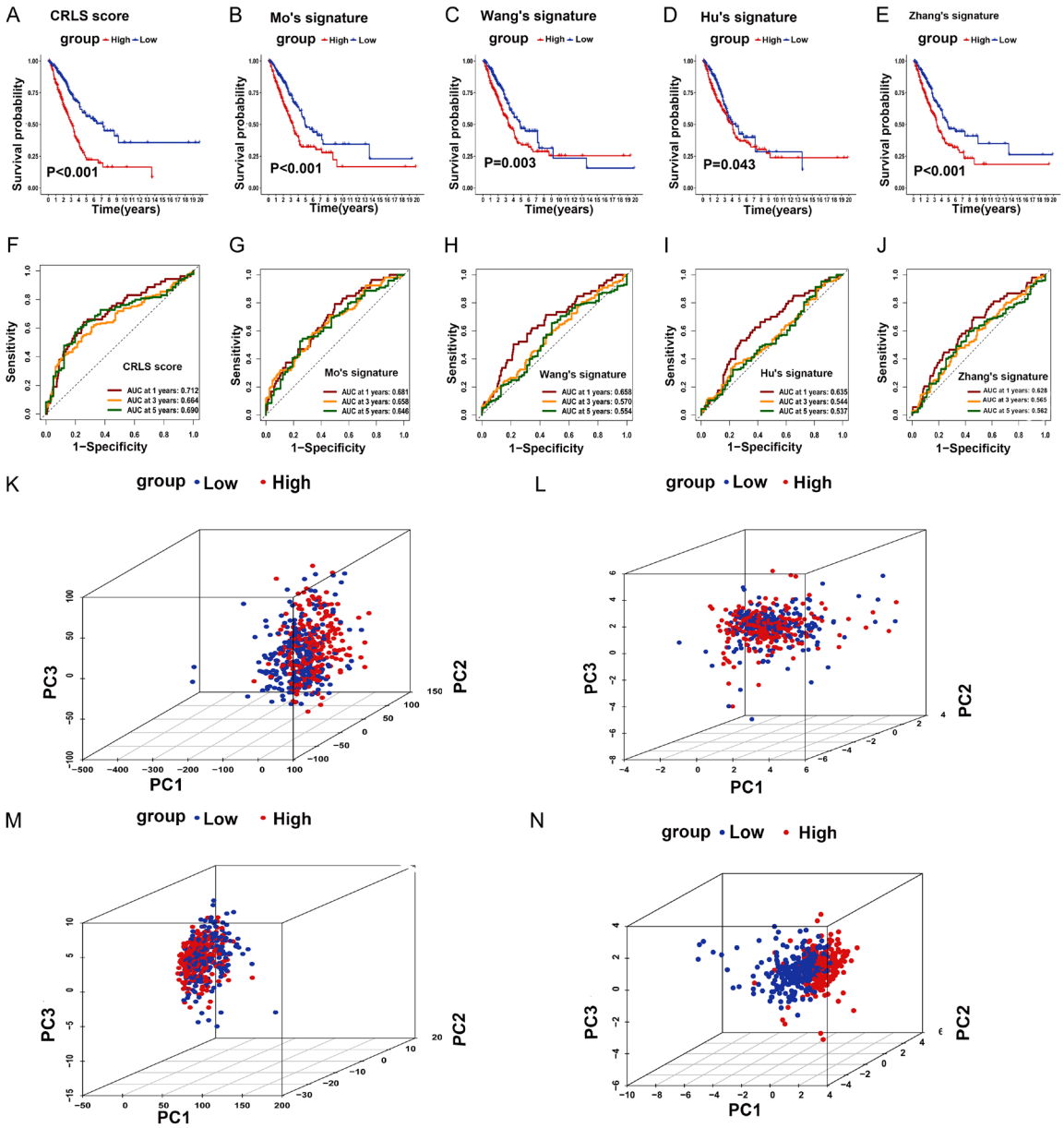


**Figure 5.** Signature comparisons and principal component analysis. (A-E) K-M analysis of CRLS (A), Mo's signature (B), Wang's signature (C), Hu's signature (D), and Zhang's signature (E) in the TCGA entire set. (F-J) ROC curves show the sensitivity and specificity of the CRLS and other 4 signatures in predicting the 1-, 3-, and 5-years OS of LUAD patients in the TCGA entire set. (K-N) PCA between the high-risk and low-risk groups based on entire gene expression profiles (K), 10 CRGs (L), 852 cuproptosis-related lncRNAs (M), and CRLS (N).

and the CRLS (**Figure 5K-N**). Using the CRLS, the distribution of the two groups was significantly different and stable. Taken together, these results demonstrated that the CRLS constructed according to the 6 cuproptosis-related lncRNAs could accurately and reliably predict the prognosis of patients with LUAD.

*Independent prognostic factor analysis and nomogram construction*

We conducted univariate and multivariate Cox regression analyses to determine whether the CRLS was an independent prognostic factor of prognosis for patients with LUAD. Univariate

Cox regression analysis showed the hazard (HR) and the 95% confidence interval (CI) of the CRLS were 1.376 and 1.203-1.575, respectively in the training set (**Figure 6A**, $P < 0.001$), and the HR of the CRLS for the testing and entire sets was 1.099 (95% CI: 1.025-1.179, $P = 0.008$) and 1.154 (95% CI: 1.090-1.221, $P < 0.001$), respectively (**Figure 6B**, **6C**). After adjusting for other confounding factors, the multivariate Cox regression analysis showed that the HR of CRLS for the training set was 1.318, with a 95% CI of 1.082-1.606 (**Figure 6D**, $P = 0.006$) and 1.092 (95% CI: 1.009-1.181, P = 0.029) and 1.131 (95% CI: 1.061-1.205, P < 0.001) for the testing and entire sets, respectively (**Figure 6E**, **6F**), indicating that our CRLS could serve as an independent prognostic risk factor for LUAD patients. Furthermore, considering the wide use of stage in clinical settings and the excellent predictive power of the CRLS, we constructed a nomogram by integrating them (**Figure 6G**), as well as calculated the individualized patient score for each patient via nomogram to better predict the prognosis of 1-, 3-, and 5-years. The subsequent calibration curve analysis further assessed the prediction accuracy of the nomogram, which demonstrated a high degree of consistency between the observed and predicted values (**Figure 6H**). Additionally, the AUCs for the 1-, 3-, and 5-years of OS were 0.843, 0.757, and 0.766, respectively, suggesting that the nomogram was reliable in predicting the prognosis of LUAD patients (**Figure 6I**). Notably, the nomogram's AUCs for predicting prognosis were also higher than that of the CRLS and other clinical factors (**Figure 6J**). In addition, the highest C-index of nomogram also indicated it had a stable and robust performance in predicting the prognosis of LUAD patients (**Figure 6K**). Together, these results demonstrated that the composite nomogram could predict the prognosis of LUAD patients accurately, which might be used in clinical to aid in treatment decision-making.

We also used the chi-square test to examine the correlation between the CRLS and clinicopathological characteristics. The strip chart indicated that the stage and T/N were significantly associated with the CRLS (Figure S2A). We then applied K-M analysis to verify whether the CRLS still possesses superior predictive power in different clinical traits and found that patients with high CRLS scores still had a similar dismal prognosis in different clinical feature groups such as age (≤ 65 or > 65 years), gender (female or male), stage (I-II or III-IV), and TNM (T1-2 or T3-4) (Figure S2B-I).

*Immune cell infiltration landscape*

Since the tumor microenvironment plays important roles in LUAD progression and treatment, we performed comprehensive analyses to investigate whether the two subgroups differed in immune cell infiltration. First, we used multiple algorithms including TIMER, CIBERSORT, xCELL, quanTIseq, MCPcounter, EPIC, and CIBESORT-ABS to assess the relationship between the CRLS and the immune cell subtype infiltration, and found a negative relationship between them (**Figure 7A**). Then, we applied the ssGSEA algorithm to investigate the infiltration of immune cell populations and immune functions in the high and low CRLS groups. The results demonstrated that the infiltration of immune cell subtypes including B cells, iDCs, Mast cells, and NK cells was significantly higher in the low CRLS group (**Figure 7B**, $P < 0.05$). In addition, the human leukocyte antigen (HLA) and type II IFN response was significantly upregulated in the low CRLS group (**Figure 7C**, $P < 0.05$). We also applied ESTIMATE algorithm to evaluate the relationship of CRLS with estimate score (**Figure 7D**), immune score (**Figure 7E**), and stromal score (**Figure 7F**), and the results was consistent with the findings above that, the CRLS scores were negatively correlated with estimate score, immune score, and stromal score. Furthermore, we examined the expression of immune checkpoint members between the high and low CRLS groups (**Figure 7G**), and of the 47 immune checkpoint members we analyzed, 16 were differentially expressed between the two groups ($P < 0.05$). Patients with low CRLS scores had significantly higher expression levels of immune checkpoint members such as CD28, BTLA, BTNL2, CD40, TNFSF14, and TNFSF9, suggesting that they might benefit more from immunotherapy. Additionally, using the immune subtype data from TIMER2.0, we tested whether the CRLS could distinguish the different immunological subtypes (**Figure 7H**). The results indicated that the CRLS had a high degree of discrimination with respect to immunological subtypes. Ac-

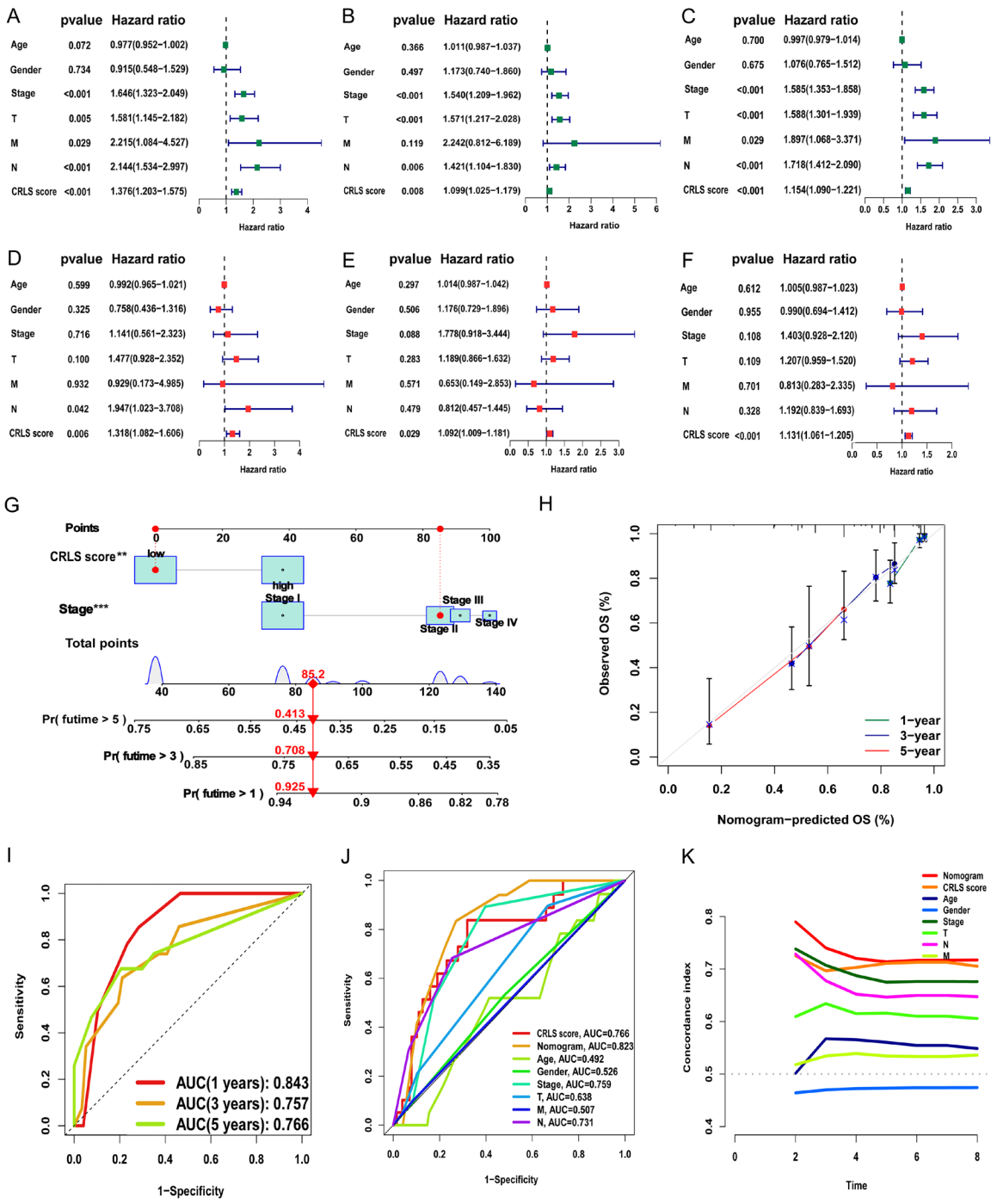


**Figure 6.** Independent prognostic factors and Nomogram construction. (A-C) The forest map of univariate based on the training (A), testing (B), and entire sets (C). (D-F) The forest map of multivariate Cox regression analysis based on the training (D), testing (E), and entire sets (F). (G) The nomogram predicts the probability of the 1-, 3-, and 5-years of OS of LUAD patients. (H) The calibration plot prediction via nomogram of the OS at 1-, 3-, and 5-year. (I) ROC curves of the nomogram for predicting the 1-, 3-, and 5-years of survival. (J) The prognostic accuracy of the nomogram, CRLS, and clinical factors was compared using time-dependent ROC curves. (K) The C-index of the nomogram, CRLS, and clinical characteristics in predicting prognosis.

cording to the above findings, patients with low CRLS scores showed higher levels of immune infiltration, which may be have contributed to their better prognosis.

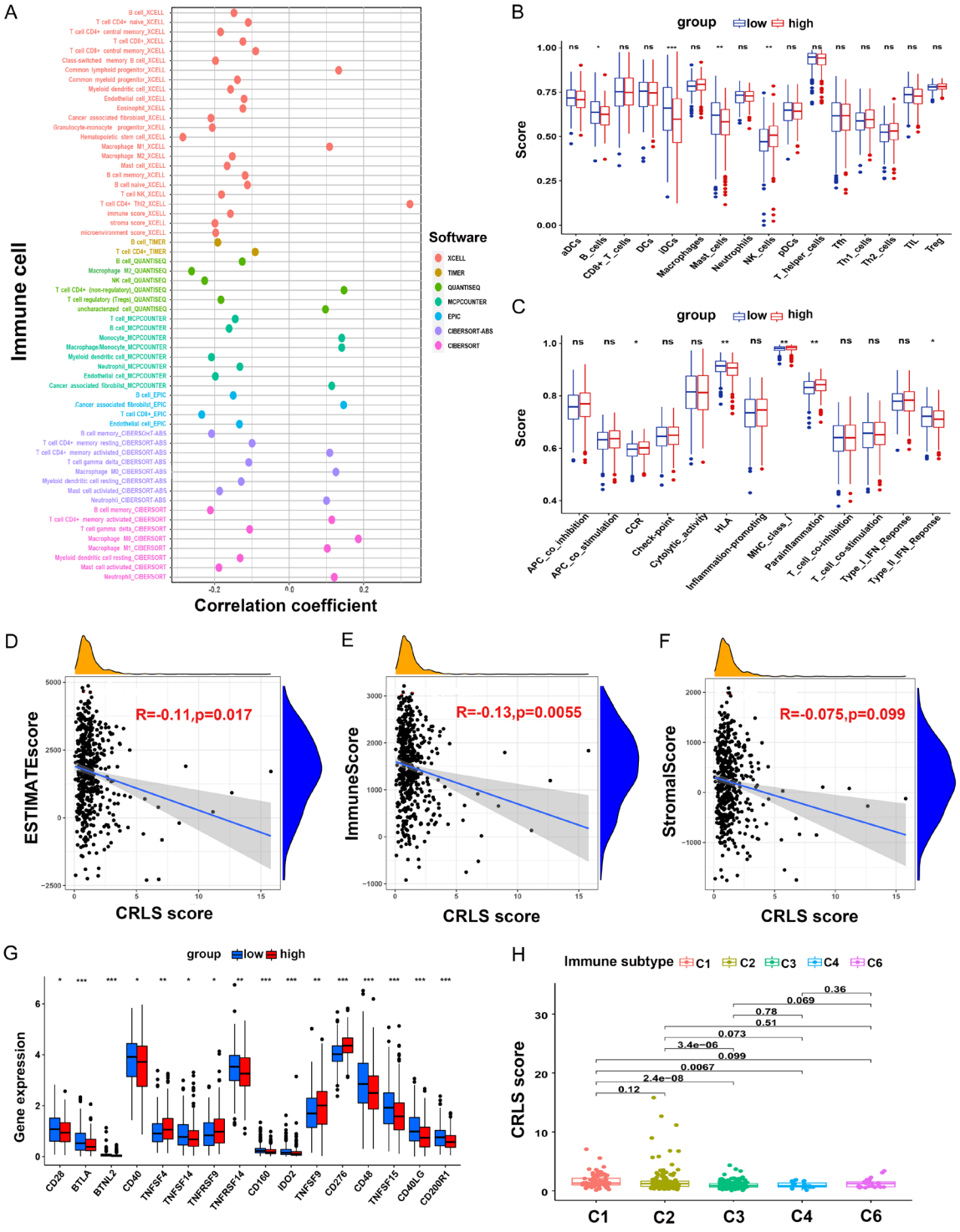


**Figure 7.** Stratification Analysis of the CRLS in immune features. (A) The relationship between the CRLS and infiltration of immune cell populations using TIMER, CIBERSORT, xCELL, quanTIseq, MCPcounter, EPIC, and CIBESORT-ABS algorithms. (B, C) The differences between the immune cell populations (B), and immune functions (C) between high CRLS and low CRLS group using the ssGSEA algorithm. (D-F) The relationship between CRLS and immune score (D), stromal score (E), and estimate score (F) using ESTIMATE algorithm. (G) The boxplot shows the expression levels of immune checkpoint members in high and low CRLS groups. (H) CRLS could accurately distinguish the different immunological subtypes (C1: Wound Healing, C2: IFN-gamma Dominant, C3: Inflammatory, C4: Lymphocyte Depleted, C5: Immunologically Quiet, C6: TGF-beta Dominant). *$P$ < 0.5, **$P$ < 0.01, ***$P$ < 0.001, ns, no sense.

*Somatic mutation landscape*

As an effective molecular marker, TMB was used to determine the quantity of mutations taken by tumor cells [21]. We then explored the difference between the high and low CRLS groups in terms of somatic mutation landscape. Waterfall plot illustrated that the mutation rates in high CRLS group (Altered in 231 (93.15%) of 248 samples) and low CRLS group (Altered in 193 (83.19%) of 232 samples), and mutation information of genes with high mutation frequency were displayed in **Figure 8A**, **8B**, respectively. Overall, frequently mutated genes such as TP53, TTN, MUC16, RYR2, CSMD3, LRP1B, ZFHX4, USH2A, and KRAS exhibited significantly higher mutational frequency in both groups. Furthermore, the TMB quantitative analysis revealed that patients with high CRLS scores had a significantly higher TMB score than patients with low CRLS scores (**Figure 8C**, $P < 0.05$). There was a positive correlation between the CRLS and the TMB according to Spearman's correlation analysis (**Figure 8D**, $R = 0.15$, $P = 0.001$). Moreover, using the median TMB score, we divided all LUAD patients into high and low TMB groups to investigate the impact of the TMB state on prognosis. K-M analysis suggested that patients with high TMB scores had better OS than patients with low TMB scores, and the difference was not statistically significant (**Figure 8E**, $P > 0.05$). Interestingly, in our subsequent analysis of predicting the outcome of LUAD patients using a combination of CRLS score and TMB, we found that patients in the group (low CRLS score and high TMB score) had significantly better prognosis than patients in all other groups, suggesting that the CRLS score was superior to the TMB in terms of predicting individual's outcome (**Figure 8F**, $P < 0.0001$). Similarly, we assessed the correlation among CRLS, TMB, and immune cell infiltration (**Figure 8G**).

*Estimation of immunotherapy response and drug sensitivity*

Furthermore, we downloaded the IPS data of patients with LUAD from (TCIA) database and evaluated the predictive value of the CRLS in IPS immunotherapy, which is a recognized model based on machine learning that predicts patients' responses to immune checkpoint blockade by estimating their immunogenicity. The results revealed a higher IPS score in the low CRLS group, suggesting that patients with low CRLS scores might respond better to immunotherapy (**Figure 9A-D**). Since chemotherapy is commonly used in LUAD treatment, we further determined how well the CRLS responded to common anti-tumor drugs. By using ridge regression, we trained the predictive model on the GDSC cell line data set with a satisfactory predictive accuracy based on a 10-fold cross validation study. Surprisingly, when comparing the IC50 values of common anti-tumor drugs in these two groups, we discovered that the low CRLS group had a higher IC50 value for targeted therapies such as erlotinib and gefitinib, as well as for chemotherapeutics such as cisplatin, paclitaxel, and gemcitabine, suggesting that patients with high CRLS scores might respond better to those drug treatment, respectively (**Figure 9E-I**). Subsequently, we screened potential therapeutic compounds for patients with high CRLS scores and found that the IC50 values of 7 compounds (A.443654, A.770041, AG.014699, AICAR, AKT.inhibitor.VIII, AUY922, AZD.0530) were significantly lower in the high CRLS group, suggesting that these drugs might be beneficial to patients with high CRLS scores (**Figure 9J-P**). By contrast, the IC50 values of 3 compounds (AS601245, ATRA, Axitinib) were significantly lower in the low CRLS group, suggesting that these drugs may be more suitable for patients with low CRLS scores (**Figure 9Q-S**).

*Functional enrichment analysis*

To understand the molecular mechanisms underlying the significant difference between the two groups in the multidimensional analysis, we performed the GO and KEGG analyses based on 216 DEGs (Table S6) between high and low CRLS groups ($|Log2FC| > 1.0$, $P$-value $< 0.05$). The GO analysis results indicated that DEGs were significantly enriched in immune-related biological processes (BP), such as antimicrobial humoral response, antibacterial humoral response, humoral immune response, and negative regulation of proteolysis (**Figure 10A**). With regard to cellular component (CC), these DEGs were significantly enriched in secretory granule lumen, collagen-containing extracellular matrix, and vesicle lumen (**Figure 10A**). As for molecular function (MF), these DEGs were significantly enriched in signaling

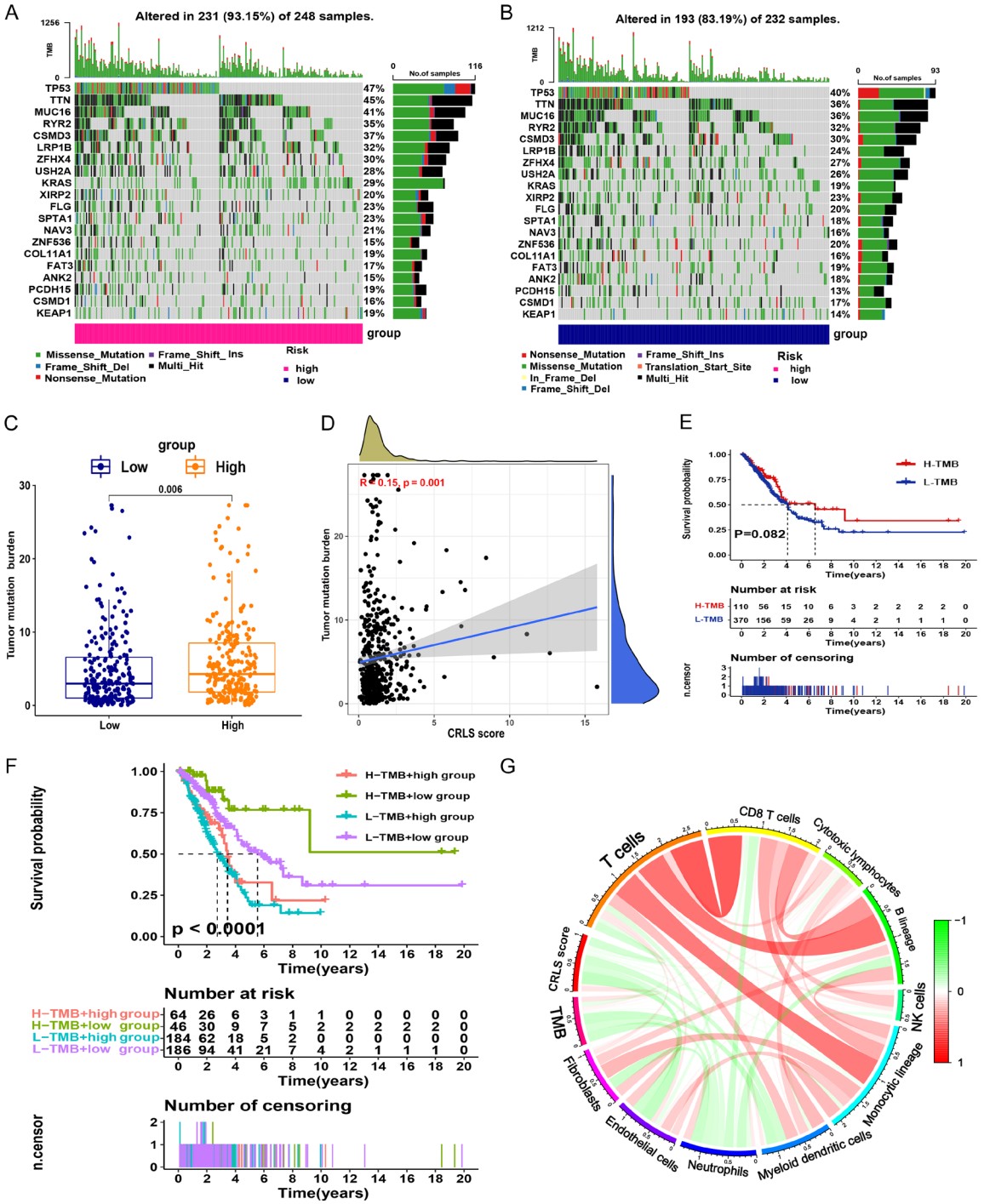


**Figure 8.** Somatic mutation landscape. (A, B) Waterfall plot displays mutation information of the 20 genes with high mutation frequencies in the high CRLS group (A) and low CRLS group (B). (C) TMB quantitative analysis. (D) The correlation between CRLS and TMB. (E, F) K-M survival curves of the OS of patients in the high-TMB and low-TMB groups (E), and patients combined with CRLS and TMB status (F). (G) The correlation analysis of the CRLS and infiltration levels of immune cells, and TMB using MCPcounter algorithm.

receptor activator activity and enzyme inhibitor activity (**Figure 10A**). Additionally, KEGG analysis indicated that these DEGs were predominantly associated with tumor-related pathways such as PI3K-Akt signaling pathway, MAPK signaling pathway, ECM-receptor interaction, and

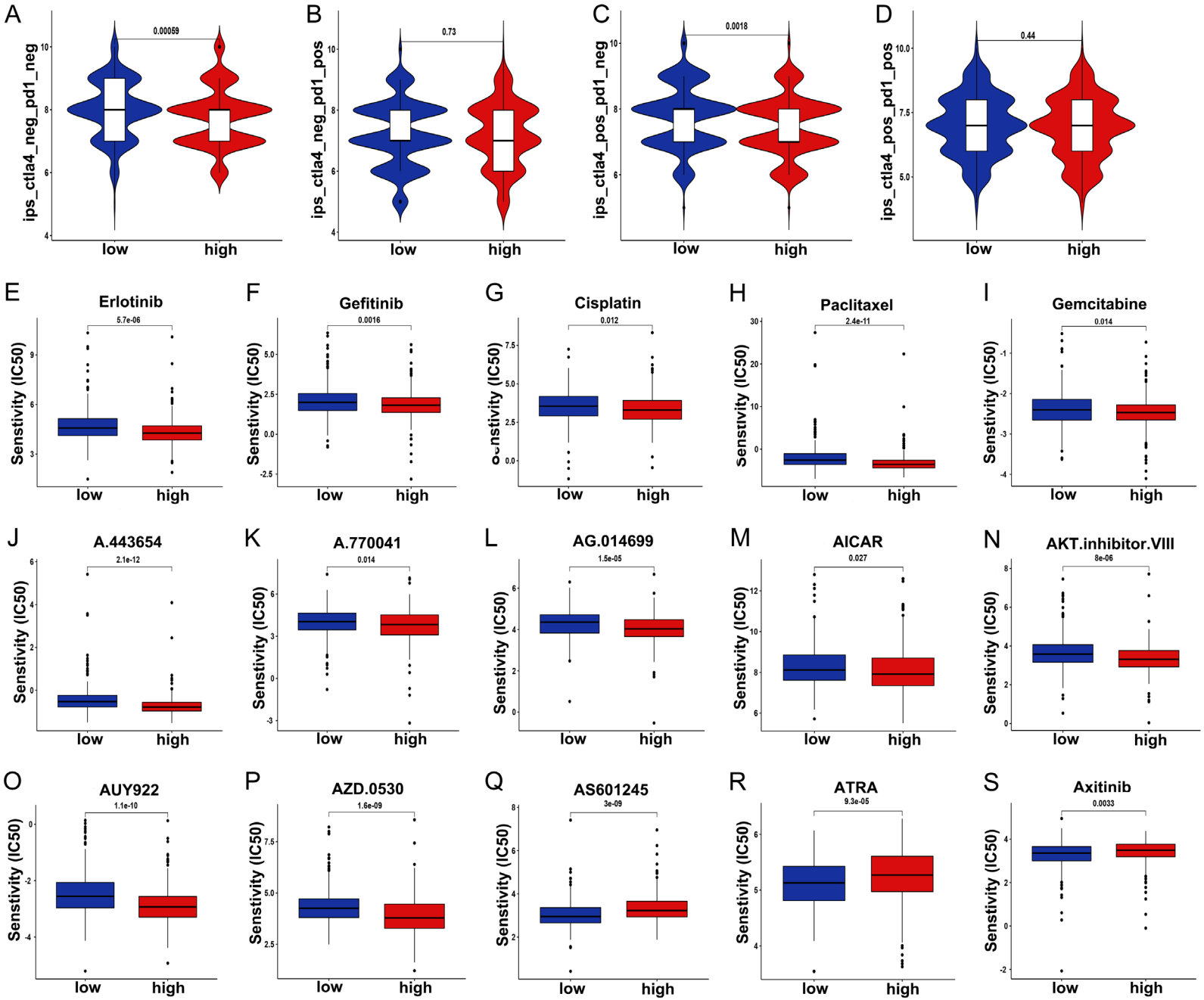
A
ips_ctla4_neg_pd1_neg
0.00059
low
high
B
ips_ctla4_neg_pd1_pos
0.73
low
high
C
ips_ctla4_pos_pd1_neg
0.0018
low
high
D
ips_ctla4_pos_pd1_pos
0.44
low
high
E
Erlotinib
5.7e-06
Senstivity (IC50)
low
high
F
Gefitinib
0.0016
Senstivity (IC50)
low
high
G
Cisplatin
0.012
Senstivity (IC50)
low
high
H
Paclitaxel
2.4e-11
Senstivity (IC50)
low
high
I
Gemcitabine
0.014
Senstivity (IC50)
low
high
J
A.443654
2.1e-12
Senstivity (IC50)
low
high
K
A.770041
0.014
Senstivity (IC50)
low
high
L
AG.014699
1.5e-05
Senstivity (IC50)
low
high
M
AICAR
0.027
Senstivity (IC50)
low
high
N
AKT.inhibitor.VIII
8e-06
Senstivity (IC50)
low
high
O
AUY922
1.1e-10
Senstivity (IC50)
low
high
P
AZD.0530
1.6e-09
Senstivity (IC50)
low
high
Q
AS601245
3e-09
Senstivity (IC50)
low
high
R
ATRA
9.3e-05
Senstivity (IC50)
low
high
S
Axitinib
0.0033
Senstivity (IC50)
low
high

**Figure 9.** Drug sensitivity and immunotherapy response analysis. (A-D) The differences of IPS_ctla4 negative_pd1 negative (A), IPS_ctla4 negative_pd1 positive (B), IPS_ctla4 positive_pd1 negative (C), and IPS_ctla4 postive_pd1 positive (D) in patients with different CRLS groups are shown. (E-I) The box plots of the estimated IC50 of patients to Erlotinib (E), Gefitinib (F), Cisplatin (G), Paclitaxel (H), and Gemcitabine (I) in high and low CRLS groups. (J-S) Screening potential drugs by targeting CRLS using the GDSC database. *$P$ < 0.5, **$P$ < 0.01, ***$P$ < 0.001, and ****P < 0.0001. ns, no sense.

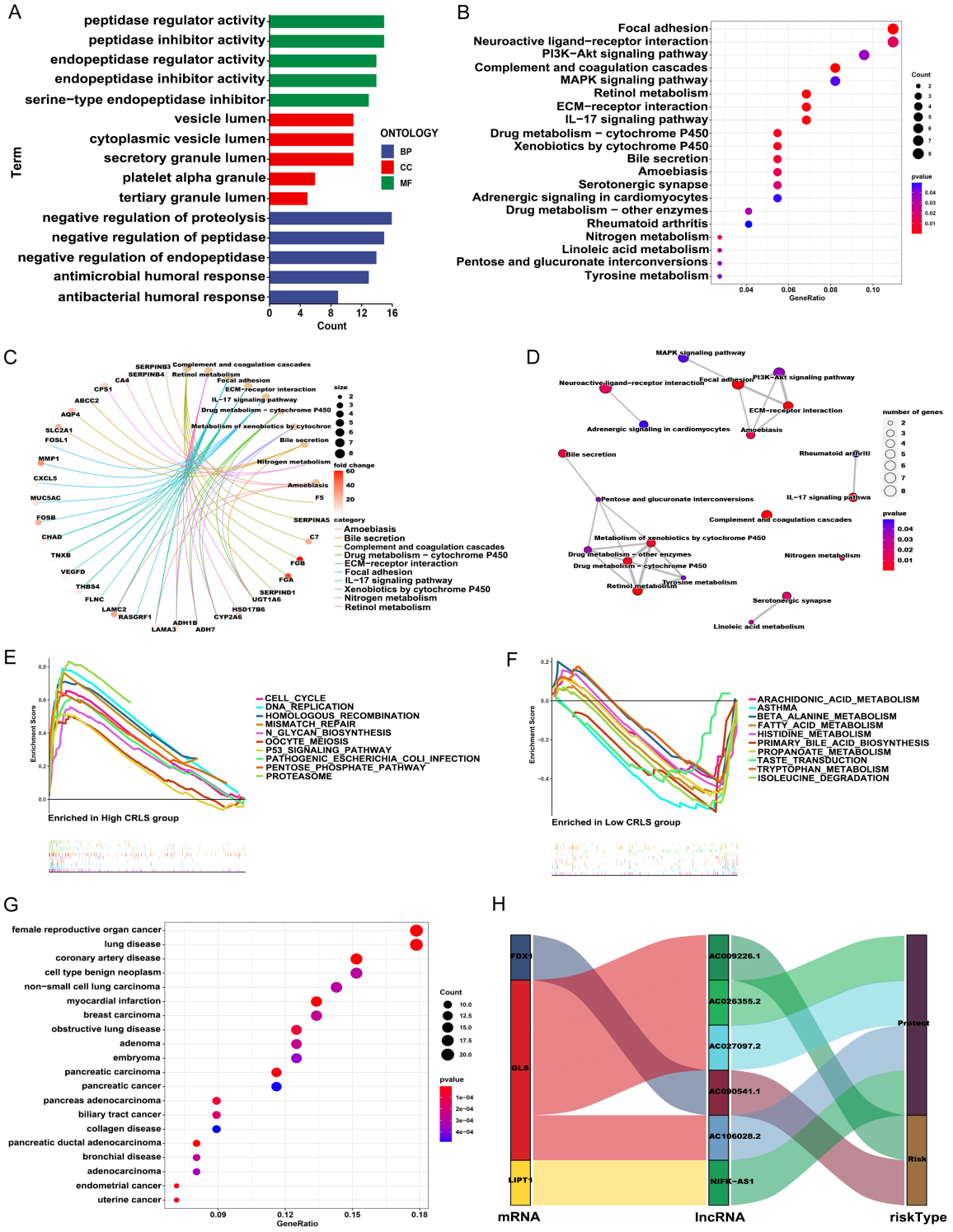

**Figure 10.** Functional analysis and visualization of lncRNAs networks. Top 10 classes of GO enrichment terms in biological process (BP), cellular component (CC), and molecular function (MF) based on DEGs between high and low CRLS groups (A). (B-D) The results of KEGG enrichment analysis based on DEGs was displayed in the bubble (B), cnet (C), and net (D). (E, F) Gene set enrichment analysis of the top 10 pathways significantly enriched in the high CRLS group (E), and in the low CRLS group (F). (G) The results of DO enrichment analysis. (H) The Sankey diagram shows the degree of connection between CRGs, six cuproptosis-related lncRNAs, and risk types.

IL-17 signaling pathway, metabolism-related pathways such as drug metabolism - cytochrome P450, and retinol metabolism (**Figure 10B-D**). Moreover, DO analysis indicated that DGEs were significantly involved in lung disease, non-small cell lung carcinoma, and other tumors (**Figure 10G**). Taken together, DEGs between high and low CRLS groups may play an important role in the pathogenesis of LUAD. Furthermore, the GSEA results revealed that the high CRLS group exhibited a significant enrichment in pathways such as cell cycle, DNA replication, homologous recombination, mismatch repair, and P53 signaling pathways (**Figure 10E**), while metabolism-related pathways such as arachidonic acid metabolism, fatty acid metabolism, and propanoate metabolism were enriched in the low CRLS group (**Figure 10F**). Furthermore, the correlation among the CRGs, the 6 lncRNAs, and the risk type was presented in the Sankey network (**Figure 10H**) [22]. The result indicated that lncRNAs AC009226.1 and AC090541.1 were risk factors, while AC027097.2, AC026355.2, NIFK-AS1, and AC106028.2 were protective factors, which was consistent with their corresponding negative/positive coefficients (Table S4).

*NIFK-AS1 regulated the proliferation and migration of LUAD cells*

To experimentally validate the findings from bioinformatics analysis, we examined the expression level of the six prognostic lncRNAs by RT-qPCR in LUAD A549 and H1975 cells, as well as in normal control BEAS-2B cell (**Figure 11A-F**). There was a significant downregulation of three lncRNAs in both LUAD cells, including NIFK-AS1, AC027097.2, and AC090541.1. Due to the fact that the high expression of lncRNAs may be associated with better survival (HR < 1) (**Figure 3G**, **3D**), and combination of the Sankey diagram (**Figure 10H**), they might serve as tumor suppressor factors. In both LUAD cells, two lncRNAs (AC009226.1, AC026355.2) were upregulated. Similarly, the high levels of expression of the two lncRNAs may be indicative of poor survival, suggesting that they might facilitate LUAD. It is interesting to note that AC106028.2 was downregulated in A549 cells, while it was upregulated in H1975 cells, which leads us to investigate the specific mechanism that causes this. Based on the bulk RNA sequencing data form TCGA database, we determined the difference in expression of these six lncRNAs in 535 LUAD samples and 59 normal tissue samples, and the expression patterns of the six lncRNAs were highly consistent with RT-qPCR (**Figure 11G**).

Since our results above showed that the expression of NIFK-AS1 was significantly different between normal and tumor samples, and there is no relevant report on NIFK-AS1 in LUAD, we chose NIFK-AS1 for further experimental verification. The expression of NIFK-AS1 was further verified in the TCGA set by using a paired t-test analysis (**Figure 11H**). In addition, we exploited the function of NIFK-AS1 in vitro in A549 cells by by cell transfection/overexpression experiments.The overexpression of NIFK-AS1 was confirmed by RT-qPCR (**Figure 11I**, $P < 0.001$). By using CCK-8 assay, we determined that NIFK-AS1 suppressed cell proliferation, which supported the finding from database analysis that NIFK-AS1 might serve as a protective factor in LUAD (**Figure 11J**, $P < 0.05$). Similarly, Overexpression of NIFK-AS1 decreased the migration of A549 cells, as determined by wound healing assay (**Figure 12A**, $P < 0.001$). In accordance with these findings, the colony formation assays also demonstrated that overexpression of NIFK-AS1 significantly decreased the viability of LUAD cells (**Figure 12B**, $P < 0.05$).

## Discussion

Induction of RCD is considered as the most promising antitumor mechanism [23, 24]. Numerous studies have demonstrated that RCDs play a significant role in the various physiological and pathological processes, including cancer; hence RCD are common targets for cancer treatment [25]. For example, Ocker et al. have shown that Bcl-2-specific siRNA that

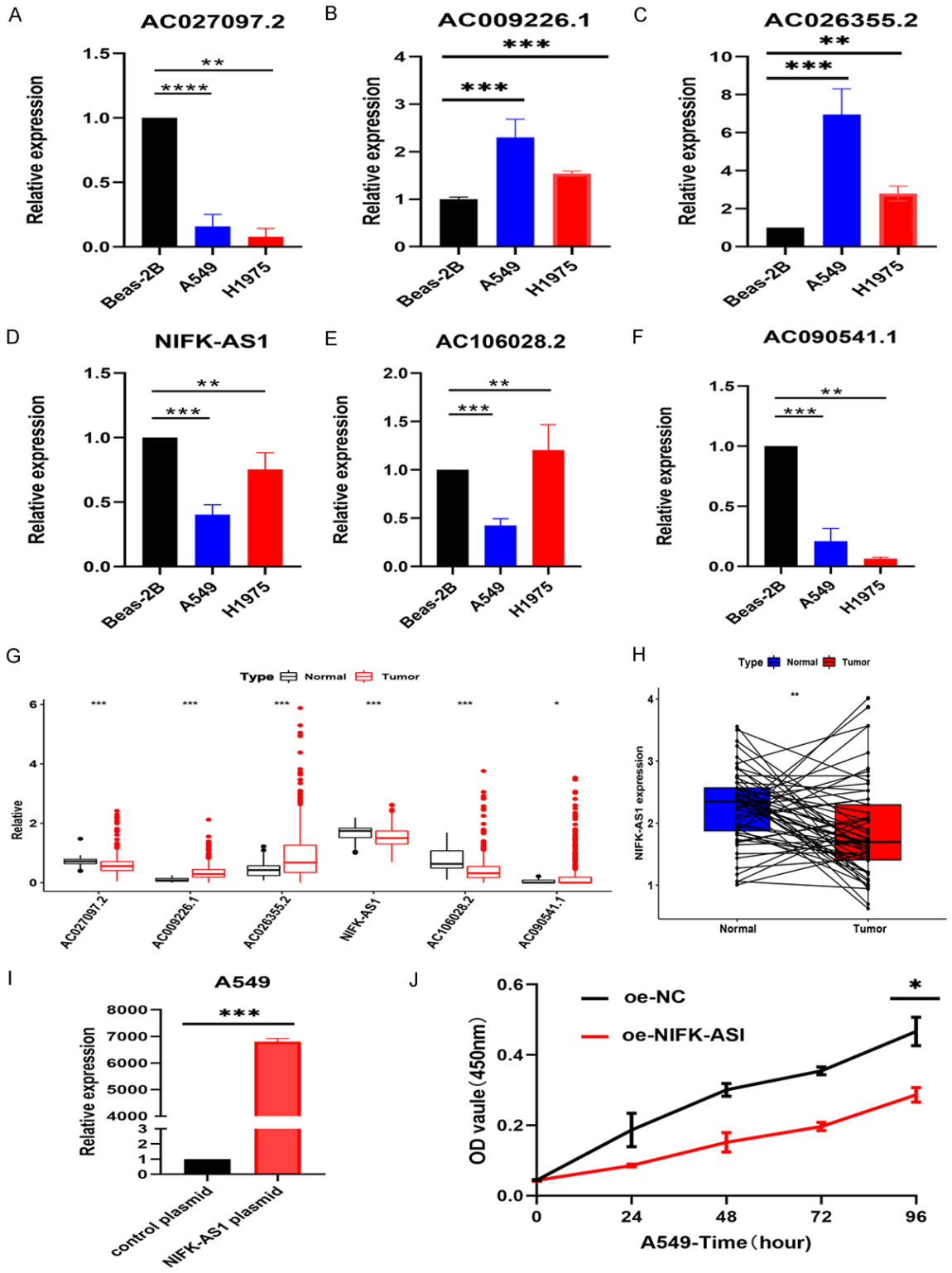


**Figure 11.** Expression levels of 6 lncRNAs and the transfection efficiency. A-F. The expression level of 6 lncRNAs between normal lung epithelial cell line (BEAS-2B) and LUAD cell lines (NCI-H1975, A549) by RT-qPCR. G. Expression levels of 6 lncRNAs between 535 LUAD and 59 normal tissues based on the TCGA databases. H. Validation of the expression levels of lncRNAs by paired analysis in the TCGA cohort. I. RT-qPCR was conducted to verify the transfection efficiency. J. The viability of A549 detected through CCK-8 assay after overexpression of NIFK-AS1. *P < 0.5, **P < 0.01, ***P < 0.001, and ****P < 0.0001. ns, no sense.

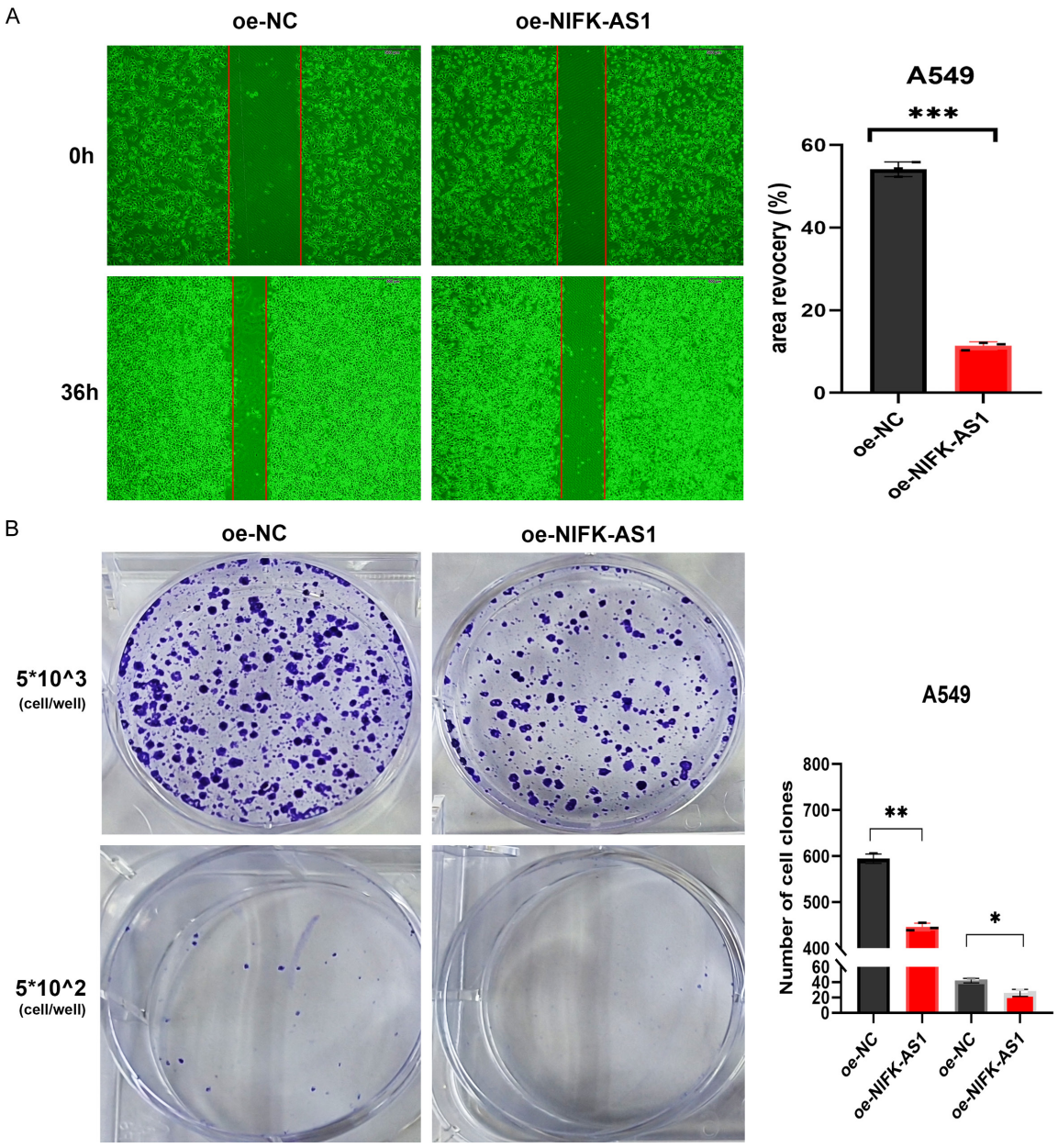


**Figure 12.** Characteristics of NIFK-AS1 and its functional effect on LUAD cells. A. Migration ability was evaluated by wound healing assay. B. Cell viability was evaluated with colony formation assays in LUAD cells. *P < 0.5, **P < 0.01, ***P < 0.001, and ****P < 0.0001. ns, no sense.

targets apoptosis can inhibit pancreatic cancer malignancy [26]. Similarly, GSDMD, a significant regulator of pyroptosis, has been found to decrease cyclin A2 and CDK2 expression, thus inhibiting tumor cell division and proliferation [27, 28]. Notably, ferroptosis is another research focus of RCD, and Abhishek et al. have reported that RCDs plays a dual role in tumor progression via ferroptosis, which may provide insight into the mechanism of RCDs [29]. It is worth mentioning that many ferroptosis-based biomarkers that can accurately predict cancer prognosis have been discovered [30, 31]. On the other hand, Tsvetkov et al. report that copper accumulation in the intracellular environment leads to the aggregation of mitochondrial acylated proteins as well as the destabilization of Fe-S cluster proteins, which ultimately results in cell death, known as cuproptosis. They identified a key regulator of cuproptosis, FDX1, as a novel effector of lipoylation, which is highly correlated with cell

survival [9]. In addition, it has been reported that lung cancer cells using galactose-mediated mitochondrial respiration are nearly 1000-fold more susceptible to growth inhibition caused by ES-Cu than those using glucose-induced glycolysis. Perhaps these mechanisms could explain the pathologies associated with inherited copper overload diseases and suggest new approaches to harness copper toxicity for cancer treatment.

Accumulating evidence has shown that in addition to protein-coding RNA mutations, mutations and abnormal modifications of non-coding RNAs represented by lncRNAs are also critical regulators in tumor progression [32]. As a result, these non-coding RNAs are regarded as new biomarkers for cancer diagnosis or therapeutic targets for cancer treatment [33-35]. In this study, we explored the connection between lncRNA and cuproptosis in predicting the survival and prognosis of LUAD patient. We identified six cuproptosis-related lncRNAs as the risk signature lncRNAs affecting the prognosis of LUAD, two of which (AC090541.1, AC009226.1) were risk factors and four of which (AC026355.2, AC027097.2, NIFK-AS1, AC106028.2) were protective factors. Actually, some of these cuproptosis-related lncRNAs have been used in constructing the prognosis prediction models for different diseases. For example, AC026355.2 has been shown to be immune-related and autophagy-related lncRNA that us related to prognosis of LUAD patients [36, 37]. There have also been many studies on NIFK-AS1. Chen et al. have revealed that NIFK-AS1 is up-regulated in hepatocellular carcinoma (HCC) and promotes HCC progression by $m^6A$ methylation [38]. In addition, Zhou et al. report that NIFK-AS1 suppresses the M2 polarization of macrophages in endometrial cancer via miR-146a activity, and a previous study confirmed that NIFK-AS1could served as a signature related to OS in glioblastoma patients [39, 40]. In this study, we not only used bioinformatics analyses but also experimentally verified the expression level of these six prognostic lncRNAs by RT-qPCR. Importantly, we were the first to demonstrate that NIFK-AS1 could significantly inhibit the growth and migration of LUAD.

It has been well known that abnormal immune cell infiltration promotes the progression of LUAD and controls the RCDs such as ferroptosis, and that checkpoint inhibitor-based immunotherapies have improved the prognosis of patients with advanced-cancer [41-44]. In this study, we found a significant difference in immune cell infiltration between the high and low CRLS groups. Compared with the high CRLS group, the infiltration of Interdigitating dendritic cells (iDCs) was significantly decreased in low CRLS group. Interestingly, Zhang et al. found that injection of remodeled iDCs combined with cisplatin into mice could significantly inhibit the growth of bladder cancer cells via the humoral immune process in xenograft tumor model [45, 46], which was consistent with our GO analysis results. Furthermore, our KEGG analysis revealed that the related functional pathways of the DEGs were mainly linked to complement and coagulation cascades, retinol metabolism, and IL-17 signaling pathway. Previous studies have shown that the differentiation of Th0 cell subsets, especially towards the Th17 cell population, is mainly regulated by interleukins (ILs) secreted by dendritic cells (DCs) [47]. In addition, Th17 cells, an important subgroup of cells differentiated from Th0 cells, play an important role in LUAD. For example, Huang Q et al. demonstrate that IL-17 can induce an endothelial-mesenchymal transition in LUAD by regulating Stat3 and can release various cellular mediators that promote LUAD invasion through Stat1 [48, 49]. In line with these studies, Chen et al. also reported that the IL-17 level in the circulating blood of LUAD patients was significantly increased [50]. The high infiltration of iDCs in LUAD as shown by our immune cell infiltration analysis and the high enrichment of the IL-17 pathway in the enrichment analysis may reveal new directions for the treatment of LUAD. Furthermore, our GSEA analysis, the high CRLS group was significantly enriched in the proteasome, cell cycle, and P53 signaling pathway, while the low CRLS group was abundant in primary bile acid biosynthesis, fatty acid metabolism, propanoate, and other metabolism pathways. Since patients in the low CRLS group showed a high immune function and immune cell infiltration, we speculate that there may be a link between immune escape and cuproptosis, which leads to a better prognosis. Further study is needed to investigate the underlying mechanisms.

We also used multiple immune-related algorithms to demonstrate that the low CRLS group was characterized by higher levels of immune cell infiltration and functions, suggesting an “immune-hot” phenotype. Consistently, we fo-

und that patients with low CRLS scores showed elevated levels of immune checkpoint members, suggesting that these patients were more likely to have better response to ICI treatment. In line with our conclusions, the result based on IPS algorithm confirmed that immunotherapy was more likely to be effective in patients with low CRLS scores. Practicing precision medicine requires clinicians to identify patients who are sensitive to different treatments as early as possible, to provide them with further treatments specific to their needs. Therefore, considering the higher sensitivity of the low CRLS group to immunotherapy, we utilized GDSC database to screen drugs beneficial for patients with high CRLS scores and found that chemotherapeutics such as cisplatin, paclitaxel, and gemcitabine, as well as targeted therapies such as erlotinib and gefitinib were more suitable for patients with high CRLS scores. We identified 7 compounds with lower IC50 value in the high CRLS group, suggesting that patients with high CRLS scores may have greater sensitivity to these drugs. Collectively, these results suggested that the prognostic signature might serve as a powerful biomarker for chemotherapy and immunotherapy.

Nevertheless, there were several limitations in our study. First, most of the approaches in this study utilized bioinformatics analysis; hence, the conclusions need to be further validated experimentally in vitro and in vivo. Second, all raw data were obtained from public databases, which might influence the results of the analysis. Using our own patient samples may help confirm the results. Lastly, cuproptosis is a newly discovered mechanism of programmed cell death with limited studies reported. There may exist more cuproptosis-related genes and lncRNAs which were missed in this study. Continuing research on this area is required.

In conclusion, we developed a robust signature called CRLS based on bioinformatics for assessing the prognosis, risk stratification, and immunotherapy response to LUAD. The CRLS demonstrated a robust predictive capability when compared with clinicopathological features. It is important to note that CRLS has important clinical implications for the management and treatment of LUAD, and patients with low CRLS scores are more sensitive to immunotherapy. Furthermore, the CRLS also appears to be a promising biomarker for predicting chemotherapy response, and some compounds may be identified as potential agents for patients with high CRLS scores. Overall, our study provides an attractive tool for the prognostic evaluation, risk stratification, and individualized treatment of LUAD patients in clinical practice.

## Disclosure of conflict of interest

None.

**Address correspondence to:** Xugang Zhong, Department of Orthopedics, Zhejiang Provincial People's Hospital, Hangzhou, Zhejiang, China; Qingdao University, Qingdao, Shandong, China. Tel: +86-17815745363; E-mail: zxg1182948991@163.com

## References

[1] Sacks D, Baxter B, Campbell BCV, Carpenter JS, Cognard C, Dippel D, Eesa M, Fischer U, Hausegger K, Hirsch JA, Shazam Hussain M, Jansen O, Jayaraman MV, Khalessi AA, Kluck BW, Lavine S, Meyers PM, Ramee S, Rüfenacht DA, Schirmer CM and Vorwerk D. Multisociety consensus quality improvement revised consensus statement for endovascular therapy of acute ischemic stroke. Int J Stroke 2018; 13: 612-632.

[2] Chen Z, Fillmore CM, Hammerman PS, Kim CF and Wong KK. Non-small-cell lung cancers: a heterogeneous set of diseases. Nat Rev Cancer 2014; 14: 535-546.

[3] Garon EB, Aerts J, Kim JS, Muehlenbein CE, Peterson P, Rizzo MT and Gadgeel SM. Safety of pemetrexed plus platinum in combination with pembrolizumab for metastatic nonsquamous non-small cell lung cancer: a post hoc analysis of KEYNOTE-189. Lung Cancer 2021; 155: 53-60.

[4] Herbst RS, Morgensztern D and Boshoff C. The biology and management of non-small cell lung cancer. Nature 2018; 553: 446-454.

[5] Osmani L, Askin F, Gabrielson E and Li QK. Current WHO guidelines and the critical role of immunohistochemical markers in the subclassification of non-small cell lung carcinoma (NSCLC): moving from targeted therapy to immunotherapy. Semin Cancer Biol 2018; 52: 103-109.

[6] Hirsch FR, Scagliotti GV, Mulshine JL, Kwon R, Curran WJ Jr, Wu YL and Paz-Ares L. Lung cancer: current therapies and new targeted treatments. Lancet 2017; 389: 299-311.

[7] Goulart BHL, Chennupati S, Fedorenko CR and Ramsey SD. Access to tyrosine kinase inhibitors and survival in patients with advanced EGFR(+) and ALK(+) positive non-small-cell lung cancer treated in the real-world. Clin Lung Cancer 2021; 22: e723-e733.

[8] Tang D, Chen X and Kroemer G. Cuproptosis: a copper-triggered modality of mitochondrial cell death. Cell Res 2022; 32: 417-418.
[9] Tsvetkov P, Coy S, Petrova B, Dreishpoon M, Verma A, Abdusamad M, Rossen J, Joesch-Cohen L, Humeidi R, Spangler RD, Eaton JK, Frenkel E, Kocak M, Corsello SM, Lutsenko S, Kanarek N, Santagata S and Golub TR. Copper induces cell death by targeting lipoylated TCA cycle proteins. Science 2022; 375: 1254-1261.
[10] Dai C, Zhao C, Xu M, Sui X, Sun L, Liu Y, Su M, Wang H, Yuan Y, Zhang S, Shi J, Sun J and Li Y. Serum lncRNAs in early pregnancy as potential biomarkers for the prediction of pregnancy-induced hypertension, including preeclampsia. Mol Ther Nucleic Acids 2021; 24: 416-425.
[11] Yan X, Hu Z, Feng Y, Hu X, Yuan J, Zhao SD, Zhang Y, Yang L, Shan W, He Q, Fan L, Kandalaft LE, Tanyi JL, Li C, Yuan CX, Zhang D, Yuan H, Hua K, Lu Y, Katsaros D, Huang Q, Montone K, Fan Y, Coukos G, Boyd J, Sood AK, Rebbeck T, Mills GB, Dang CV and Zhang L. Comprehensive genomic characterization of long non-coding RNAs across human cancers. Cancer Cell 2015; 28: 529-540.
[12] Wang M, Mao C, Ouyang L, Liu Y, Lai W, Liu N, Shi Y, Chen L, Xiao D, Yu F, Wang X, Zhou H, Cao Y, Liu S, Yan Q, Tao Y and Zhang B. Long noncoding RNA LINC00336 inhibits ferroptosis in lung cancer by functioning as a competing endogenous RNA. Cell Death Differ 2019; 26: 2329-2343.
[13] Yu L, Qiao R, Xu J, Han B and Zhong R. FAM207BP, a pseudogene-derived lncRNA, facilitates proliferation, migration and invasion of lung adenocarcinoma cells and acts as an immune-related prognostic factor. Life Sci 2021; 268: 119022.
[14] Mao C, Wang X, Liu Y, Wang M, Yan B, Jiang Y, Shi Y, Shen Y, Liu X, Lai W, Yang R, Xiao D, Cheng Y, Liu S, Zhou H, Cao Y, Yu W, Muegge K, Yu H and Tao Y. A G3BP1-Interacting lncRNA promotes ferroptosis and apoptosis in cancer via nuclear sequestration of p53. Cancer Res 2018; 78: 3484-3496.
[15] Friedman J, Hastie T and Tibshirani R. Regularization paths for generalized linear models via coordinate descent. J Stat Softw 2010; 33: 1-22.
[16] Calling S, Johansson SE, Wolff M, Sundquist J and Sundquist K. Total cholesterol/HDL-C ratio versus non-HDL-C as predictors for ischemic heart disease: a 17-year follow-up study of women in southern Sweden. BMC Cardiovasc Disord 2021; 21: 163.
[17] Vidaurre D. A new model for simultaneous dimensionality reduction and time-varying functional connectivity estimation. PLoS Comput Biol 2021; 17: e1008580.
[18] Newman AM, Liu CL, Green MR, Gentles AJ, Feng W, Xu Y, Hoang CD, Diehn M and Alizadeh AA. Robust enumeration of cell subsets from tissue expression profiles. Nat Methods 2015; 12: 453-457.
[19] Shen S, Wang G, Zhang R, Zhao Y, Yu H, Wei Y and Chen F. Development and validation of an immune gene-set based Prognostic signature in ovarian cancer. EBioMedicine 2019; 40: 318-326.
[20] Kong KE, Fischer B, Meurer M, Kats I, Li Z, Rühle F, Barry JD, Kirrmaier D, Chevyreva V, San Luis BJ, Costanzo M, Huber W, Andrews BJ, Boone C, Knop M and Khmelinskii A. Timer-based proteomic profiling of the ubiquitin-proteasome system reveals a substrate receptor of the GID ubiquitin ligase. Mol Cell 2021; 81: 2460-2476, e2411.
[21] Chan TA, Yarchoan M, Jaffee E, Swanton C, Quezada SA, Stenzinger A and Peters S. Development of tumor mutation burden as an immunotherapy biomarker: utility for the oncology clinic. Ann Oncol 2019; 30: 44-56.
[22] Wu Q, Li Q, Zhu W, Zhang X and Li H. Identification of autophagy-related long non-coding RNA prognostic signature for breast cancer. J Cell Mol Med 2021; 25: 4088-4098.
[23] Chen X, Zeh HJ, Kang R, Kroemer G and Tang D. Cell death in pancreatic cancer: from pathogenesis to therapy. Nat Rev Gastroenterol Hepatol 2021; 18: 804-823.
[24] Su Z, Yang Z, Xu Y, Chen Y and Yu Q. Apoptosis, autophagy, necroptosis, and cancer metastasis. Mol Cancer 2015; 14: 48.
[25] Koren E and Fuchs Y. Modes of regulated cell death in cancer. Cancer Discov 2021; 11: 245-265.
[26] Ocker M, Neureiter D, Lueders M, Zopf S, Ganslmayer M, Hahn EG, Herold C and Schuppan D. Variants of bcl-2 specific siRNA for silencing antiapoptotic bcl-2 in pancreatic cancer. Gut 2005; 54: 1298-1308.
[27] Oakes V, Wang W, Harrington B, Lee WJ, Beamish H, Chia KM, Pinder A, Goto H, Inagaki M, Pavey S and Gabrielli B. Cyclin A/Cdk2 regulates Cdh1 and claspin during late S/G2 phase of the cell cycle. Cell Cycle 2014; 13: 3302-3311.
[28] Gopinathan L, Tan SL, Padmakumar VC, Coppola V, Tessarollo L and Kaldis P. Loss of Cdk2 and cyclin A2 impairs cell proliferation and tumorigenesis. Cancer Res 2014; 74: 3870-3879.
[29] Garg AD and Agostinis P. Cell death and immunity in cancer: from danger signals to mimicry of pathogen defense responses. Immunol Rev 2017; 280: 126-148.
[30] Liu Y, Zhang X, Zhang J, Tan J, Li J and Song Z. Development and validation of a combined ferroptosis and immune prognostic classifier for

hepatocellular carcinoma. Front Cell Dev Biol 2020; 8: 596679.
[31] Zhuo S, Chen Z, Yang Y, Zhang J, Tang J and Yang K. Clinical and biological significances of a ferroptosis-related gene signature in glioma. Front Oncol 2020; 10: 590861.
[32] Bhan A, Soleimani M and Mandal SS. Long Noncoding RNA and cancer: a new paradigm. Cancer Res 2017; 77: 3965-3981.
[33] Kong X, Duan Y, Sang Y, Li Y, Zhang H, Liang Y, Liu Y, Zhang N and Yang Q. LncRNA-CDC6 promotes breast cancer progression and function as ceRNA to target CDC6 by sponging microRNA-215. J Cell Physiol 2019; 234: 9105-9117.
[34] Xing C, Sun SG, Yue ZQ and Bai F. Role of lncRNA LUCAT1 in cancer. Biomed Pharmacother 2021; 134: 111158.
[35] Wang L, Cho KB, Li Y, Tao G, Xie Z and Guo B. Long Noncoding RNA (lncRNA)-mediated competing endogenous RNA networks provide novel potential biomarkers and therapeutic targets for colorectal cancer. Int J Mol Sci 2019; 20: 5758.
[36] Gong Z, Li Q, Li J, Xie J and Wang W. A novel signature based on autophagy-related lncRNA for prognostic prediction and candidate drugs for lung adenocarcinoma. Transl Cancer Res 2022; 11: 14-28.
[37] He C, Yin H, Zheng J, Tang J, Fu Y and Zhao X. Identification of immune-associated lncRNAs as a prognostic marker for lung adenocarcinoma. Transl Cancer Res 2021; 10: 998-1012.
[38] Chen YT, Xiang D, Zhao XY and Chu XY. Upregulation of lncRNA NIFK-AS1 in hepatocellular carcinoma by m(6)A methylation promotes disease progression and sorafenib resistance. Hum Cell 2021; 34: 1800-1811.
[39] Zhou YX, Zhao W, Mao LW, Wang YL, Xia LQ, Cao M, Shen J and Chen J. Long non-coding RNA NIFK-AS1 inhibits M2 polarization of macrophages in endometrial cancer through targeting miR-146a. Int J Biochem Cell Biol 2018; 104: 25-33.
[40] Santangelo A, Rossato M, Lombardi G, Benfatto S, Lavezzari D, De Salvo GL, Indraccolo S, Dechecchi MC, Prandini P, Gambari R, Scapoli C, Di Gennaro G, Caccese M, Eoli M, Rudà R, Brandes AA, Ibrahim T, Rizzato S, Lolli I, Lippi G, Delledonne M, Zagonel V and Cabrini G. A molecular signature associated with prolonged survival in glioblastoma patients treated with regorafenib. Neuro Oncol 2021; 23: 264-276.
[41] Biton J, Mansuet-Lupo A, Pécuchet N, Alifano M, Ouakrim H, Arrondeau J, Boudou-Rouquette P, Goldwasser F, Leroy K, Goc J, Wislez M, Germain C, Laurent-Puig P, Dieu-Nosjean MC, Cremer I, Herbst R, Blons H and Damotte D. TP53, STK11, and EGFR mutations predict tumor immune profile and the response to anti-PD-1 in lung adenocarcinoma. Clin Cancer Res 2018; 24: 5710-5723.
[42] Kang L, Miao MS, Song YG, Fang XY, Zhang J, Zhang YN and Miao JX. Total flavonoids of Taraxacum mongolicum inhibit non-small cell lung cancer by regulating immune function. J Ethnopharmacol 2021; 281: 114514.
[43] Wang W, Green M, Choi JE, Gijón M, Kennedy PD, Johnson JK, Liao P, Lang X, Kryczek I, Sell A, Xia H, Zhou J, Li G, Li J, Li W, Wei S, Vatan L, Zhang H, Szeliga W, Gu W, Liu R, Lawrence TS, Lamb C, Tanno Y, Cieslik M, Stone E, Georgiou G, Chan TA, Chinnaiyan A and Zou W. CD8(+) T cells regulate tumour ferroptosis during cancer immunotherapy. Nature 2019; 569: 270-274.
[44] Lang X, Green MD, Wang W, Yu J, Choi JE, Jiang L, Liao P, Zhou J, Zhang Q, Dow A, Saripalli AL, Kryczek I, Wei S, Szeliga W, Vatan L, Stone EM, Georgiou G, Cieslik M, Wahl DR, Morgan MA, Chinnaiyan AM, Lawrence TS and Zou W. Radiotherapy and immunotherapy promote tumoral lipid oxidation and ferroptosis via synergistic repression of SLC7A11. Cancer Discov 2019; 9: 1673-1685.
[45] Zhang Q and Chen Z. Sensitization of cisplatin resistant bladder tumor by combination of cisplatin treatment and co-culture of dendritic cells with apoptotic bladder cancer cells. Cell Mol Biol (Noisy-le-grand) 2018; 64: 102-107.
[46] Gil Del Alcazar CR, Huh SJ, Ekram MB, Trinh A, Liu LL, Beca F, Zi X, Kwak M, Bergholtz H, Su Y, Ding L, Russnes HG, Richardson AL, Babski K, Min Hui Kim E, McDonnell CH 3rd, Wagner J, Rowberry R, Freeman GJ, Dillon D, Sorlie T, Coussens LM, Garber JE, Fan R, Bobolis K, Allred DC, Jeong J, Park SY, Michor F and Polyak K. Immune escape in breast cancer during in situ to invasive carcinoma transition. Cancer Discov 2017; 7: 1098-1115.
[47] Sutton CE, Lalor SJ, Sweeney CM, Brereton CF, Lavelle EC and Mills KH. Interleukin-1 and IL-23 induce innate IL-17 production from gammadelta T cells, amplifying Th17 responses and autoimmunity. Immunity 2009; 31: 331-341.
[48] Huang Q, Han J, Fan J, Duan L, Guo M, Lv Z, Hu G, Chen L, Wu F, Tao X, Xu J and Jin Y. IL-17 induces EMT via Stat3 in lung adenocarcinoma. Am J Cancer Res 2016; 6: 440-451.
[49] Wu F, Xu J, Huang Q, Han J, Duan L, Fan J, Lv Z, Guo M, Hu G, Chen L, Zhang S, Tao X, Ma W and Jin Y. The role of interleukin-17 in lung cancer. Mediators Inflamm 2016; 2016: 8494079.
[50] Chen G, Zhang PG, Li JS, Duan JJ, Su W, Guo SP, Wang YF, Sun JN and Yang XT. Th17 cell frequency and IL-17A production in peripheral blood of patients with non-small-cell lung cancer. J Int Med Res 2020; 48: 300060520925948.

**Table S1.** Ten Cuproptosis associated genes

| |
|---|
| FDX1 |
| LIAS |
| LIPT1 |
| DLD |
| DLAT |
| PDHA1 |
| PDHB |
| MTF1 |
| GLS |
| CDKN2A |

**Table S3.** The clinical and pathological characteristics of LUAD samples betwenn training and testing set

| Covariates | Type | Total | Test | Train | *P* value |
|---|---|---|---|---|---|
| Age | ≤ 65 | 231 (47.14%) | 109 (44.67%) | 122 (49.59%) | 0.3133 |
| Age | > 65 | 249 (50.82%) | 130 (53.28%) | 119 (48.37%) | |
| Age | unknow | 10 (2.04%) | 5 (2.05%) | 5 (2.03%) | |
| Gender | FEMALE | 262 (53.47%) | 125 (51.23%) | 137 (55.69%) | 0.3684 |
| | MALE | 228 (46.53%) | 119 (48.77%) | 109 (44.31%) | |
| Stage | Stage I | 4 (0.82%) | 2 (0.82%) | 2 (0.81%) | 0.1747 |
| | Stage IA | 128 (26.12%) | 61 (25%) | 67 (27.24%) | |
| | Stage IB | 131 (26.73%) | 63 (25.82%) | 68 (27.64%) | |
| | Stage II | 1 (0.2%) | 0 (0%) | 1 (0.41%) | |
| | Stage IIA | 48 (9.8%) | 26 (10.66%) | 22 (8.94%) | |
| | Stage IIB | 66 (13.47%) | 30 (12.3%) | 36 (14.63%) | |
| | Stage IIIA | 69 (14.08%) | 40 (16.39%) | 29 (11.79%) | |
| | Stage IIIB | 10 (2.04%) | 9 (3.69%) | 1 (0.41%) | |
| | Stage IV | 25 (5.1%) | 10 (4.1%) | 15 (6.1%) | |
| | unknow | 8 (1.63%) | 3 (1.23%) | 5 (2.03%) | |
| T | T1 | 163 (33.27%) | 79 (32.38%) | 84 (34.15%) | 0.9435 |
| | T2 | 263 (53.67%) | 131 (53.69%) | 132 (53.66%) | |
| | T3 | 43 (8.78%) | 22 (9.02%) | 21 (8.54%) | |
| | T4 | 18 (3.67%) | 10 (4.1%) | 8 (3.25%) | |
| | unknow | 3 (0.61%) | 2 (0.82%) | 1 (0.41%) | |
| M | M0 | 324 (66.12%) | 163 (66.8%) | 161 (65.45%) | 0.5449 |
| | M1 | 24 (4.9%) | 10 (4.1%) | 14 (5.69%) | |
| | unknow | 142 (28.98%) | 71 (29.1%) | 71 (28.86%) | |
| N | N0 | 317 (64.69%) | 146 (59.84%) | 171 (69.51%) | 0.02 |
| | N1 | 92 (18.78%) | 46 (18.85%) | 46 (18.7%) | |
| | N2 | 68 (13.88%) | 44 (18.03%) | 24 (9.76%) | |
| | N3 | 2 (0.41%) | 2 (0.82%) | 0 (0%) | |
| | unknow | 11 (2.24%) | 6 (2.46%) | 5 (2.03%) | |

**Table S4.** Multivariate Cox analysis of identifying 6 cuproptosis-related lncRNAs associated with OS

| id | coef | HR | HR.95L | HR.95H | *p* value |
|---|---|---|---|---|---|
| AC090541.1 | 0.487818878 | 1.580318312 | 1.114357892 | 2.241116598 | 0.0102452 |
| AC027097.2 | -0.802318637 | 0.30543264 | 0.107115683 | 0.870919131 | 0.0265221 |
| AC009226.1 | 1.620721254 | 2.883964024 | 1.265747771 | 6.571015712 | 0.0117072 |
| AC026355.2 | -0.365560906 | 0.670110361 | 0.483638931 | 0.928477564 | 0.0161292 |
| NIFK-AS1 | -0.546026685 | 0.454920902 | 0.227267884 | 0.910612722 | 0.0261206 |
| AC106028.2 | -0.875355074 | 0.379919531 | 0.180605412 | 0.79919449 | 0.0107494 |

**Table S5.** 4 Cuproptosis-related published signatures for LUAD retrieved from *Pubmed*

| DOI/PMID | Author'name | Title |
|---|---|---|
| DOI: 10.3389/fonc.2022.927706 | Xiaocong Mo | A novel cuproptosis-related prognostic lncRNA signature and lncRNA MIR31HG/miR-193a-3p/TNFRSF21 regulatory axis in lung adenocarcinoma. |
| DOI: 10.3389/fphar.2022.971867 | Shaohui Wang | Comprehensive bioinformatics analysis to identify a novel cuproptosis-related prognostic signature and its ceRNA regulatory axis and candidate traditional Chinese medicine active ingredients in lung adenocarcinoma. |
| DOI: 10.3389/fonc.2022.922332 | Qin Hu | Cuproptosis predicts the risk and clinical outcomes of lung adenocarcinoma. |
| DOI: 10.3389/fgene.2022.975185 | Huizhe Zhang | A novel defined cuproptosis-related gene signature for predicting the prognosis of lung adenocarcinoma. |

**Table S6.** 216 DEGs between high-risk and low-risk groups

| gene | low Mean | high Mean | logFC | *p* Value | fdr |
|---|---|---|---|---|---|
| SNORA12 | 12.554466 | 1.3908997 | -3.17411 | 0.0105132 | 0.0229547 |
| LRRK2-DT | 5.1972051 | 1.6634657 | -1.643544 | 3.44E-16 | 1.63E-13 |
| IGF2BP3 | 1.1446794 | 2.3030654 | 1.0086119 | 4.54E-11 | 1.78E-09 |
| QPCT | 12.628837 | 26.46936 | 1.0676015 | 6.03E-10 | 1.58E-08 |
| SNORA74B | 5.7929987 | 0.5947283 | -3.284008 | 0.0011529 | 0.0035607 |
| TCF21 | 2.1526368 | 0.9156882 | -1.233177 | 1.08E-07 | 1.37E-06 |
| MYEOV | 2.8758027 | 8.2561694 | 1.5215079 | 2.56E-09 | 5.47E-08 |
| SBSN | 0.6783333 | 1.4634717 | 1.1093285 | 0.0001416 | 0.0005969 |
| PI3 | 9.193196 | 47.165238 | 2.3590855 | 0.0008718 | 0.0027953 |
| CHIA | 5.3654356 | 1.3742804 | -1.965019 | 6.17E-08 | 8.62E-07 |
| GLB1L3 | 3.9439339 | 1.589997 | -1.310611 | 3.08E-07 | 3.34E-06 |
| EPS8L3 | 1.4403725 | 2.9829725 | 1.0503087 | 3.14E-06 | 2.42E-05 |
| SFTPC | 554.55525 | 143.80689 | -1.947198 | 3.11E-07 | 3.36E-06 |
| AGTR2 | 4.1363351 | 1.4191421 | -1.543334 | 3.33E-05 | 0.0001745 |
| LAMA3 | 5.0491547 | 10.396921 | 1.0420426 | 0.0061159 | 0.014476 |
| TFF1 | 51.870329 | 150.77255 | 1.5393924 | 1.14E-05 | 7.11E-05 |
| RASGRF1 | 2.7314417 | 1.2663465 | -1.10899 | 4.62E-08 | 6.80E-07 |
| AC116407.1 | 1.9441544 | 0.9272213 | -1.068157 | 1.01E-14 | 1.84E-12 |
| AC018629.1 | 0.5823111 | 1.4985095 | 1.3636662 | 0.0002617 | 0.0010015 |
| RNU7-45P | 3.6160911 | 1.5225211 | -1.247969 | 0.0025071 | 0.006798 |
| NR4A1AS | 2.1507996 | 0.8489085 | -1.341192 | 4.10E-09 | 8.29E-08 |
| TFF2 | 26.431584 | 71.399303 | 1.4336471 | 0.0248331 | 0.0470414 |
| GJB2 | 10.76029 | 22.028512 | 1.0336551 | 1.59E-11 | 7.35E-10 |
| IL1A | 0.4629445 | 1.6555307 | 1.8383826 | 0.0004646 | 0.0016347 |

| | | | | | |
|---|---|---|---|---|---|
| HSD17B13 | 1.9801842 | 0.6813221 | -1.539226 | 3.85E-11 | 1.54E-09 |
| PEBP4 | 27.481336 | 9.4142971 | -1.545527 | 3.05E-11 | 1.26E-09 |
| MMP10 | 2.8648443 | 7.9013833 | 1.4636485 | 0.0001594 | 0.0006578 |
| UGT1A6 | 1.2804815 | 2.7627251 | 1.1094056 | 0.026384 | 0.0494565 |
| LHFPL3-AS2 | 4.0634418 | 1.8309849 | -1.150082 | 4.89E-06 | 3.48E-05 |
| S100P | 119.73626 | 262.62226 | 1.1331291 | 0.0009839 | 0.0031037 |
| ADRB1 | 1.934137 | 0.9639754 | -1.004622 | 7.55E-08 | 1.02E-06 |
| GPR35 | 1.3467212 | 2.7423829 | 1.0259788 | 2.39E-07 | 2.70E-06 |
| MIR23A | 1.6118317 | 0.7918887 | -1.025332 | 3.39E-05 | 0.0001773 |
| AL663070.1 | 2.1348874 | 1.0641487 | -1.00446 | 2.21E-09 | 4.86E-08 |
| LAMC2 | 28.730705 | 70.591354 | 1.2968981 | 3.70E-14 | 4.80E-12 |
| CRYM | 10.531967 | 5.1349174 | -1.036362 | 5.29E-08 | 7.58E-07 |
| SCARNA7 | 12.377246 | 3.2580262 | -1.92562 | 0.0016741 | 0.0048602 |
| SLC2A1 | 25.629815 | 51.866426 | 1.0169779 | 8.22E-16 | 3.30E-13 |
| FOSB | 25.653508 | 12.492393 | -1.038106 | 8.75E-05 | 0.0003964 |
| MUC5AC | 10.555916 | 25.287117 | 1.2603509 | 0.0010271 | 0.0032251 |
| TNS4 | 4.236414 | 12.061959 | 1.5095487 | 6.10E-06 | 4.19E-05 |
| MIR3677 | 2.44758 | 1.126257 | -1.11982 | 2.93E-10 | 8.49E-09 |
| HSD17B6 | 14.575291 | 6.8922363 | -1.080481 | 2.39E-09 | 5.17E-08 |
| GKN2 | 13.780944 | 5.1940573 | -1.407741 | 3.24E-07 | 3.49E-06 |
| CPS1 | 15.243074 | 35.947652 | 1.2377437 | 0.0047827 | 0.0117438 |
| RTN4RL1 | 1.8498489 | 0.9004542 | -1.038683 | 1.03E-09 | 2.53E-08 |
| BTNL9 | 1.797246 | 0.7342522 | -1.29144 | 7.34E-13 | 5.53E-11 |
| MS4A2 | 1.5005489 | 0.738874 | -1.02209 | 5.49E-07 | 5.55E-06 |
| KHDRBS2 | 1.4758503 | 0.6569942 | -1.167594 | 9.48E-11 | 3.34E-09 |
| SERPINB4 | 0.7619746 | 1.5529386 | 1.027186 | 0.0001445 | 0.000607 |
| IGF2BP1 | 0.5552202 | 1.6408248 | 1.5632892 | 1.05E-10 | 3.68E-09 |
| VIL1 | 2.878833 | 5.8068562 | 1.0122732 | 1.06E-05 | 6.67E-05 |
| AQP4 | 21.613312 | 8.4646396 | -1.3524 | 3.32E-14 | 4.49E-12 |
| AC012511.1 | 1.6206427 | 0.7948127 | -1.027879 | 2.51E-12 | 1.60E-10 |
| PRSS3 | 0.9995 | 3.9036083 | 1.9655298 | 0.0002697 | 0.0010269 |
| CA4 | 1.5218137 | 0.5777537 | -1.397265 | 0.0006299 | 0.0021186 |
| HP | 32.398743 | 12.318736 | -1.395084 | 0.0004266 | 0.0015205 |
| SERPINB5 | 2.3183757 | 6.4033684 | 1.4657166 | 6.30E-08 | 8.78E-07 |
| LGI3 | 1.893044 | 0.5102726 | -1.891368 | 6.87E-07 | 6.73E-06 |
| SNORA20 | 3.0849451 | 0.5791249 | -2.413298 | 0.0131425 | 0.027671 |
| AC026785.3 | 1.2277828 | 2.5453095 | 1.0517857 | 0.0001049 | 0.0004639 |
| RNU6-1016P | 3.426798 | 1.6239825 | -1.077325 | 0.0016012 | 0.0046732 |
| DKK1 | 5.1537022 | 11.624699 | 1.1735123 | 7.99E-06 | 5.25E-05 |
| AL049555.1 | 0.885438 | 1.9498207 | 1.1388783 | 0.0029263 | 0.0077494 |
| F5 | 1.9561323 | 4.283175 | 1.1306767 | 9.82E-07 | 9.07E-06 |
| MS4A1 | 4.65706 | 1.9963312 | -1.222068 | 2.36E-05 | 0.000131 |
| LINC01655 | 2.5368762 | 1.1734587 | -1.112286 | 3.06E-09 | 6.36E-08 |
| LINC00973 | 0.7131625 | 2.5869633 | 1.8589567 | 0.000649 | 0.0021718 |
| PGC | 1241.4095 | 420.15966 | -1.56297 | 1.19E-07 | 1.50E-06 |
| ARNTL2 | 3.2616762 | 7.1560651 | 1.1335529 | 1.92E-13 | 1.83E-11 |
| AGER | 54.315356 | 22.699714 | -1.258686 | 1.02E-07 | 1.31E-06 |
| AC092071.1 | 3.6933606 | 1.3612764 | -1.439974 | 2.75E-13 | 2.48E-11 |
| IGFBP1 | 0.5035461 | 4.961795 | 3.3006664 | 1.40E-05 | 8.51E-05 |

| | | | | | |
|---|---|---|---|---|---|
| STC1 | 5.9233227 | 12.007297 | 1.0194328 | 7.32E-08 | 9.97E-07 |
| POPDC3 | 0.8273033 | 1.6821055 | 1.0237799 | 0.001398 | 0.0041748 |
| RN7SL381P | 2.8570836 | 1.1900877 | -1.263475 | 0.0030836 | 0.0080974 |
| SERPINA5 | 0.7726695 | 1.6078507 | 1.0572101 | 0.0008788 | 0.0028108 |
| CYP2A6 | 3.2246446 | 1.3477954 | -1.258539 | 4.30E-06 | 3.11E-05 |
| MIR3671 | 1.5986172 | 0.7276825 | -1.135444 | 3.16E-11 | 1.29E-09 |
| RPL26P30 | 1.4475579 | 0.6648998 | -1.122412 | 1.28E-10 | 4.32E-09 |
| CXCL5 | 5.1592313 | 12.420506 | 1.2674959 | 1.30E-05 | 7.97E-05 |
| FLNC | 2.1681958 | 4.5030571 | 1.0544097 | 1.55E-07 | 1.85E-06 |
| WFDC5 | 5.6096835 | 0.2552621 | -4.457868 | 0.0006034 | 0.0020466 |
| MALAT1 | 135.60403 | 36.194504 | -1.905557 | 3.52E-07 | 3.74E-06 |
| AC105118.1 | 1.5604315 | 0.5838962 | -1.418161 | 0.0018961 | 0.0054031 |
| ARL14 | 1.8711598 | 3.9488766 | 1.0775095 | 1.31E-05 | 8.07E-05 |
| SHISA3 | 19.347616 | 9.522553 | -1.022735 | 0.0040737 | 0.0102612 |
| SNORA22C | 2.324367 | 0.2572141 | -3.175796 | 0.0097138 | 0.0214708 |
| RNU6-247P | 1.6496123 | 0.5427203 | -1.603846 | 0.0003326 | 0.00123 |
| KLK6 | 1.7061678 | 8.3477389 | 2.290626 | 8.02E-07 | 7.70E-06 |
| VGF | 1.4164623 | 3.8288515 | 1.4346195 | 0.0001292 | 0.0005528 |
| KLF15 | 4.0548374 | 1.9943264 | -1.023743 | 1.50E-11 | 7.01E-10 |
| SFTA1P | 36.358867 | 16.461911 | -1.143175 | 8.60E-14 | 9.27E-12 |
| PLA2G4F | 3.4810798 | 1.7061141 | -1.028821 | 1.36E-10 | 4.52E-09 |
| ECRG4 | 1.9260136 | 0.9119668 | -1.078565 | 1.31E-08 | 2.28E-07 |
| HHIP | 2.1413959 | 0.947839 | -1.175838 | 2.41E-07 | 2.71E-06 |
| AC079467.1 | 1.9449266 | 0.6553287 | -1.569425 | 1.27E-09 | 3.04E-08 |
| CPAMD8 | 4.4968069 | 1.9155336 | -1.231155 | 1.19E-14 | 2.00E-12 |
| B4GALNT2 | 0.4222264 | 1.6513967 | 1.9675982 | 0.0037606 | 0.0095837 |
| AL162511.1 | 5.6065216 | 1.7131193 | -1.71048 | 4.95E-14 | 5.97E-12 |
| AKR1B15 | 0.8211096 | 1.6903595 | 1.0416834 | 0.0016419 | 0.0047771 |
| ADAMTS8 | 1.7225863 | 0.6932878 | -1.31305 | 5.74E-11 | 2.16E-09 |
| ITLN1 | 46.273418 | 0.6803985 | -6.08766 | 0.0006382 | 0.0021401 |
| GJB3 | 2.9524244 | 7.9352292 | 1.4263718 | 1.07E-09 | 2.61E-08 |
| SPINK13 | 2.6708535 | 1.067355 | -1.323261 | 0.0102261 | 0.0224089 |
| WIF1 | 24.626419 | 9.8182567 | -1.326668 | 2.40E-09 | 5.17E-08 |
| C7 | 25.768197 | 11.238764 | -1.197108 | 8.45E-09 | 1.57E-07 |
| ADH7 | 1.7187873 | 0.570932 | -1.59 | 0.0176005 | 0.0352569 |
| MMP1 | 34.587565 | 88.415417 | 1.3540445 | 6.81E-07 | 6.67E-06 |
| MSTN | 2.5183274 | 0.0592111 | -5.410454 | 4.61E-07 | 4.74E-06 |
| TMEM130 | 6.4403168 | 2.5508311 | -1.336164 | 1.99E-09 | 4.45E-08 |
| AKAP12 | 4.1049319 | 11.358737 | 1.4683722 | 3.81E-05 | 0.0001962 |
| TAC4 | 2.8380589 | 1.1871651 | -1.257384 | 2.03E-06 | 1.68E-05 |
| ZNF385B | 4.3479121 | 1.9167967 | -1.181625 | 4.17E-09 | 8.39E-08 |
| FGB | 61.307841 | 140.2777 | 1.1941422 | 0.0018562 | 0.00531 |
| CYP24A1 | 16.320714 | 35.613696 | 1.125728 | 1.11E-07 | 1.41E-06 |
| CHRDL1 | 7.7632482 | 3.3193132 | -1.225776 | 5.25E-11 | 2.00E-09 |
| HTR1D | 0.7823238 | 1.6815679 | 1.1039693 | 4.57E-11 | 1.78E-09 |
| THBS4 | 8.0880731 | 2.0974292 | -1.947174 | 2.96E-05 | 0.0001582 |
| RN7SL8P | 2.4271278 | 0.7215568 | -1.750065 | 2.07E-05 | 0.0001174 |
| HHIP-AS1 | 3.2316582 | 1.5521062 | -1.058047 | 1.55E-10 | 5.03E-09 |
| LINC01116 | 0.8115015 | 1.7704599 | 1.1254585 | 8.59E-05 | 0.0003904 |

| | | | | | |
|---|---|---|---|---|---|
| INMT | 12.057792 | 5.0299482 | -1.26135 | 1.68E-11 | 7.62E-10 |
| AC022784.1 | 1.0027718 | 2.3017638 | 1.1987465 | 1.79E-07 | 2.10E-06 |
| CDH17 | 2.2773041 | 5.3210746 | 1.2243906 | 0.0005057 | 0.0017561 |
| SOSTDC1 | 1.800882 | 0.6267708 | -1.522694 | 1.01E-09 | 2.49E-08 |
| ADGRF4 | 1.1202729 | 2.7758687 | 1.3090891 | 5.17E-17 | 3.81E-14 |
| RNU4-1 | 61.540757 | 7.0487854 | -3.126096 | 0.0256935 | 0.0483973 |
| VEGFD | 3.6120014 | 1.281242 | -1.495255 | 1.79E-10 | 5.62E-09 |
| SERPINB3 | 2.6501456 | 6.3428631 | 1.2590626 | 0.0026609 | 0.0071407 |
| SPINK5 | 9.5401457 | 4.539154 | -1.071588 | 0.0001294 | 0.0005532 |
| KLK8 | 0.9602025 | 2.6790204 | 1.4802949 | 0.0014803 | 0.0043743 |
| SNORA22 | 4.8470253 | 0.8354903 | -2.536405 | 0.0140926 | 0.0293355 |
| FGA | 54.775436 | 158.46204 | 1.5325363 | 0.0229215 | 0.0439666 |
| LRRK2 | 11.315506 | 4.6649107 | -1.27838 | 2.52E-12 | 1.60E-10 |
| SERPIND1 | 10.310291 | 3.6665797 | -1.491578 | 3.34E-06 | 2.54E-05 |
| MELTF | 2.1413876 | 4.4126753 | 1.0431076 | 2.81E-10 | 8.24E-09 |
| SLC16A11 | 2.0700887 | 0.9260229 | -1.160573 | 2.14E-08 | 3.46E-07 |
| ANXA10 | 3.1940162 | 9.4857964 | 1.5703973 | 0.0010094 | 0.0031723 |
| PCSK2 | 21.506904 | 3.3151486 | -2.697654 | 0.0005275 | 0.0018241 |
| PTHLH | 1.3454939 | 3.2003452 | 1.2500916 | 1.12E-09 | 2.71E-08 |
| SUSD2 | 57.424083 | 18.768965 | -1.613307 | 5.01E-14 | 5.98E-12 |
| AC027288.2 | 1.9957555 | 0.5612701 | -1.830168 | 3.23E-15 | 8.30E-13 |
| MIR3189 | 8.9397593 | 3.4477541 | -1.374579 | 1.99E-08 | 3.27E-07 |
| RNU5F-1 | 1.7966965 | 0.5259898 | -1.77224 | 0.0011918 | 0.0036614 |
| MIR6071 | 1.5576235 | 0.7718226 | -1.013005 | 5.06E-07 | 5.16E-06 |
| ESYT3 | 2.8993432 | 1.3170156 | -1.138454 | 1.95E-19 | 1.09E-15 |
| C5orf38 | 6.3558205 | 3.1689885 | -1.004056 | 8.25E-13 | 6.15E-11 |
| GAL | 1.0735143 | 4.6129314 | 2.1033425 | 4.07E-08 | 6.06E-07 |
| KRT6A | 20.610398 | 46.520025 | 1.1744795 | 2.89E-06 | 2.26E-05 |
| MAMDC2 | 3.8030818 | 1.8494042 | -1.040108 | 1.43E-08 | 2.46E-07 |
| RHCG | 0.4862769 | 1.9420196 | 1.9977076 | 0.0145946 | 0.0301955 |
| CNMD | 19.203849 | 3.3289554 | -2.528254 | 4.09E-05 | 0.0002084 |
| SNORA53 | 13.478657 | 2.0801279 | -2.695933 | 0.0032626 | 0.008494 |
| CYP4B1 | 47.415053 | 16.027185 | -1.564824 | 2.64E-17 | 2.70E-14 |
| ADH1B | 11.612727 | 3.7643266 | -1.625243 | 4.64E-12 | 2.65E-10 |
| TPSD1 | 2.4250188 | 1.11469 | -1.121353 | 2.62E-05 | 0.0001425 |
| FAM83A | 13.072623 | 34.800777 | 1.4125709 | 7.78E-15 | 1.47E-12 |
| SLC15A1 | 0.6277636 | 1.4429507 | 1.2007286 | 0.0141184 | 0.0293799 |
| PI15 | 0.8481836 | 2.6670032 | 1.652771 | 0.0078342 | 0.0179412 |
| AL021068.1 | 2.3903855 | 0.8973105 | -1.413564 | 0.0200355 | 0.0393296 |
| CACNA2D2 | 15.095576 | 6.0422511 | -1.320968 | 3.55E-17 | 3.14E-14 |
| REG4 | 5.2267421 | 29.131043 | 2.4785735 | 0.0169221 | 0.0341428 |
| PRG4 | 9.8306188 | 0.9383055 | -3.389153 | 1.22E-07 | 1.52E-06 |
| PAEP | 35.17575 | 92.648256 | 1.3971826 | 0.0002904 | 0.0010911 |
| AC026355.2 | 1.9513116 | 0.737301 | -1.404119 | 1.99E-14 | 3.00E-12 |
| AC007552.2 | 1.5851101 | 0.7850974 | -1.013639 | 6.10E-06 | 4.19E-05 |
| LINC01843 | 0.7333915 | 1.5044016 | 1.0365344 | 1.36E-07 | 1.67E-06 |
| C2orf72 | 0.951965 | 2.1733802 | 1.1909602 | 5.90E-05 | 0.0002835 |
| FAM177B | 1.1790779 | 2.5549644 | 1.1156442 | 0.0025339 | 0.0068624 |
| OGN | 3.2819836 | 1.3480826 | -1.283659 | 5.54E-06 | 3.86E-05 |

| | | | | | |
|---|---|---|---|---|---|
| GDF10 | 2.0325266 | 0.9030675 | -1.170369 | 5.29E-07 | 5.36E-06 |
| LRRC36 | 1.5773748 | 0.5264268 | -1.583221 | 2.83E-10 | 8.29E-09 |
| ALOX15 | 3.3059764 | 1.6343542 | -1.016356 | 0.0203023 | 0.039765 |
| AKR1B10 | 22.147528 | 76.483462 | 1.7880022 | 0.0018067 | 0.0051909 |
| AL355916.1 | 0.7947226 | 1.6913443 | 1.089647 | 0.0134103 | 0.028136 |
| Z83843.1 | 2.5598032 | 1.2132814 | -1.077119 | 1.80E-08 | 3.00E-07 |
| SLPI | 1022.7974 | 397.16627 | -1.364705 | 1.33E-06 | 1.17E-05 |
| KRT20 | 2.2703332 | 18.574804 | 3.0323711 | 0.009351 | 0.0208215 |
| LINC00460 | 1.5454568 | 3.2672958 | 1.0800638 | 0.0025782 | 0.0069638 |
| FOSL1 | 4.1253602 | 10.272738 | 1.3162288 | 7.17E-11 | 2.63E-09 |
| SNORA73B | 196.26129 | 26.168991 | -2.906845 | 0.0004205 | 0.0015035 |
| SCARNA13 | 18.827383 | 3.1126003 | -2.59664 | 4.63E-06 | 3.31E-05 |
| CLIC5 | 5.8575068 | 2.5291342 | -1.211643 | 2.33E-10 | 7.05E-09 |
| COLCA1 | 3.3752507 | 1.5986336 | -1.078155 | 1.30E-10 | 4.37E-09 |
| SNORA26 | 5.1141103 | 2.4216783 | -1.078476 | 0.0016768 | 0.004867 |
| AC092279.2 | 1.425843 | 0.6869953 | -1.053443 | 1.64E-12 | 1.13E-10 |
| LINC02471 | 1.646685 | 0.7038939 | -1.226135 | 6.20E-06 | 4.24E-05 |
| CDA | 11.822335 | 24.295352 | 1.0391654 | 3.24E-07 | 3.48E-06 |
| TNXB | 2.3977531 | 1.0779741 | -1.153361 | 1.17E-05 | 7.28E-05 |
| CD109 | 2.7920849 | 5.7072351 | 1.0314491 | 5.28E-10 | 1.41E-08 |
| TRIM31 | 1.9220979 | 4.6880778 | 1.2863147 | 0.0003505 | 0.0012902 |
| RHOV | 12.228973 | 27.771478 | 1.1833007 | 2.60E-06 | 2.06E-05 |
| SCGB3A2 | 593.80555 | 144.64547 | -2.037469 | 8.12E-12 | 4.13E-10 |
| HMGA2 | 0.5503288 | 1.8164684 | 1.7227705 | 1.16E-06 | 1.04E-05 |
| ABCC2 | 1.8590294 | 5.6023832 | 1.5914911 | 0.0046697 | 0.0115003 |
| AC120498.2 | 1.5297799 | 0.6202431 | -1.302418 | 3.88E-07 | 4.06E-06 |
| TCN1 | 9.9186948 | 27.59207 | 1.4760315 | 2.22E-09 | 4.86E-08 |
| C16orf89 | 174.31993 | 71.423921 | -1.287258 | 2.15E-14 | 3.16E-12 |
| GGTLC1 | 20.680863 | 8.0586747 | -1.359682 | 1.77E-14 | 2.71E-12 |
| AC090181.2 | 1.9276554 | 0.943554 | -1.03067 | 9.66E-06 | 6.19E-05 |
| LYPD3 | 4.5839095 | 11.736278 | 1.3563245 | 2.92E-06 | 2.27E-05 |
| SYT13 | 2.0427987 | 5.1582424 | 1.3363325 | 3.37E-05 | 0.0001766 |
| WFDC12 | 5.3578748 | 0.2518313 | -4.411131 | 0.0001397 | 0.0005912 |
| RN7SKP80 | 2.0985802 | 0.6879872 | -1.60896 | 3.56E-09 | 7.28E-08 |
| LINC02257 | 3.6647095 | 1.8305824 | -1.001396 | 2.04E-09 | 4.54E-08 |
| MUC6 | 13.504322 | 4.9953824 | -1.434754 | 0.0232677 | 0.0445424 |
| GNG4 | 1.5512255 | 3.2110985 | 1.0496584 | 2.78E-07 | 3.07E-06 |
| SCGB3A1 | 876.58009 | 213.43244 | -2.038106 | 4.48E-10 | 1.23E-08 |
| SFTPD | 238.85205 | 99.594168 | -1.261984 | 1.11E-11 | 5.49E-10 |
| CHAD | 4.551707 | 1.5427551 | -1.560899 | 4.77E-10 | 1.29E-08 |
| SLC46A2 | 3.723101 | 1.452267 | -1.358198 | 1.56E-10 | 5.05E-09 |
| FAM83A-AS1 | 1.8100679 | 4.2094319 | 1.2175817 | 4.90E-09 | 9.64E-08 |
| MACROD2 | 2.9382344 | 1.3806832 | -1.089567 | 7.56E-07 | 7.31E-06 |
| INSL4 | 1.2023521 | 4.1136862 | 1.7745723 | 0.0004252 | 0.0015168 |
| RNU4ATAC | 2.5965684 | 0.5402918 | -2.264795 | 1.04E-05 | 6.59E-05 |

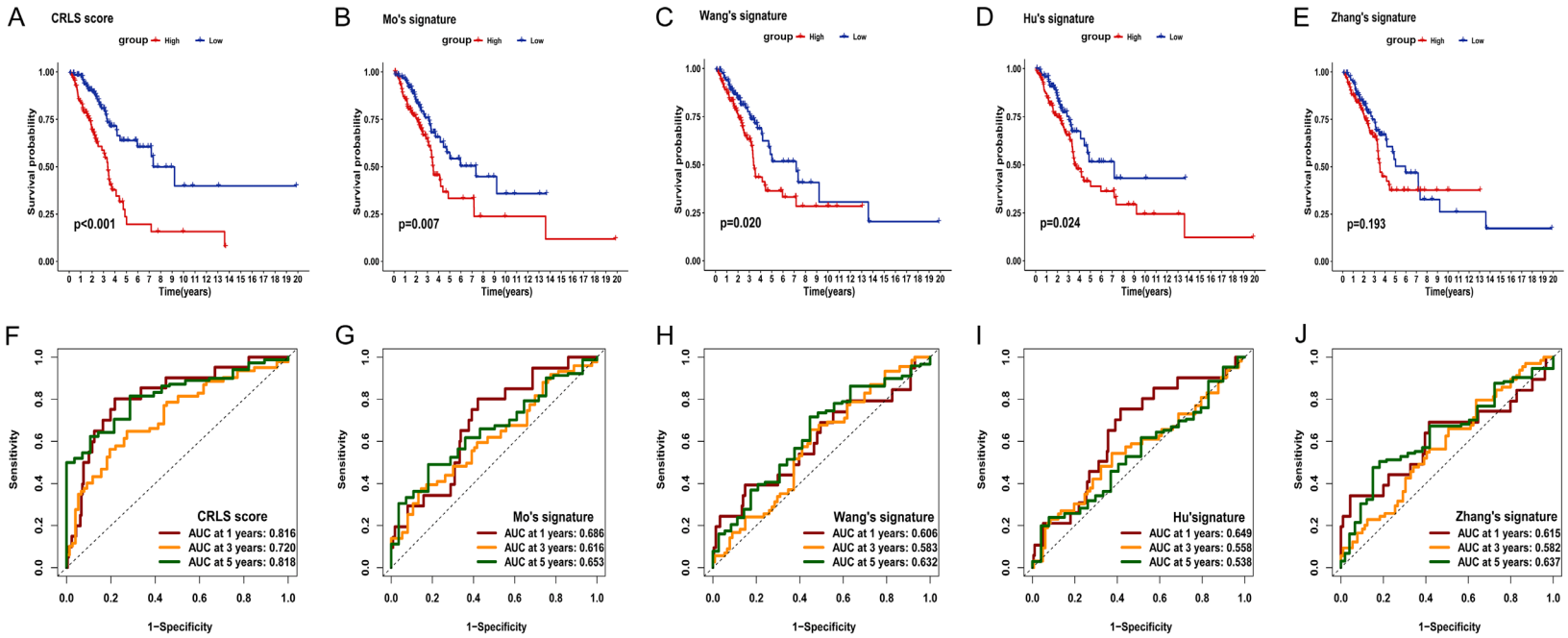


**Figure S1.** Signature comparisons. (A-E) K-M analysis of CRLS (A), Mo's signature (B), Wang's signature (C), Hu's signature (D), and Zhang's signature (E) in the training set. (F-J) ROC curves show the sensitivity and specificity of the CRLS (F), Mo's signature (G), Wang's signature (H), Hu's signature (I), and Zhang's signature (J) in predicting the 1-, 3-, and 5-years OS of LUAD patients in the training set.

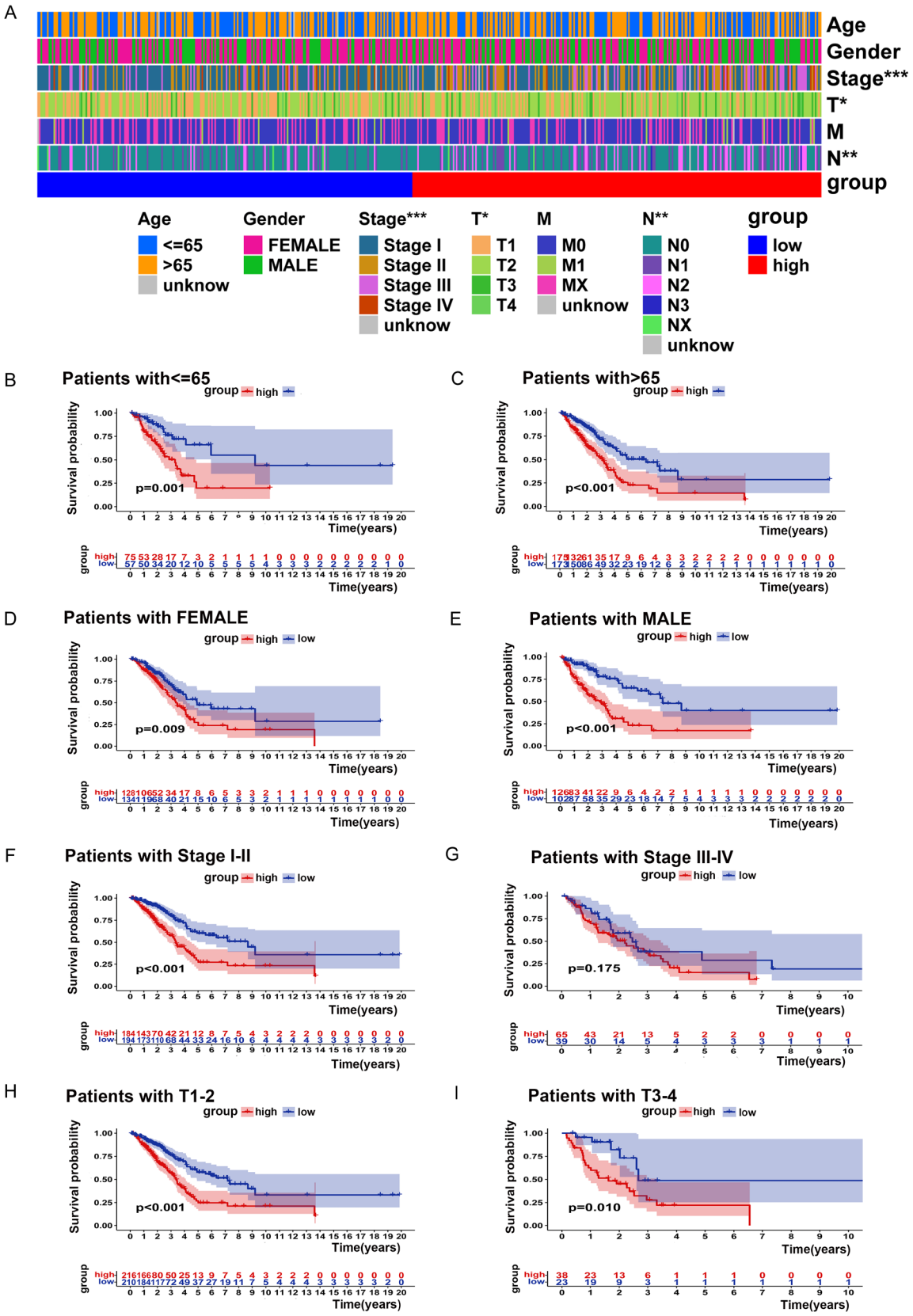


**Figure S2.** Clinical characteristic evaluation by using the CRLS. (A) A hot plot of clinical characteristics and CRLS. (B-I) Kaplan-Meier curves of OS difference stratified by age (B, C), gender (D, E), stage (F, G), and TNM (H, I) between the high CRLS and low CRLS groups in the TCGA entire set.